Pergamon

Geochimica et Cosmochimica Acta, Vol. xx, No. x, pp. xxx, 2004

0016-7037/04 $30.00 + .00

doi:10.1016/j.gca.2004.05.027

The dissolution rates of natural glasses as a function of their composition at pH 4 and 10.6, and temperatures from 25 to 74°C

DOMENIK WOLFF-BOENISCH,[1,*] SIGURDUR R. GISLASON,[1] ERIC H. OELKERS[2] and CHRISTINE V. PUTNIS[3]

[1]Science Institute, University of Iceland, Dunhagi 3, 107 Reykjavik, Iceland.
[2]Géochimie: Transferts et Mécanismes, CNRS/UMR 5563–Université Paul Sabatier, 38 rue des Trente-six Ponts, 31400 Toulouse, France.
[3]Institut für Mineralogie, Westfälische Wilhelms-Universität, Corrensstr. 24, 48149 Münster, Germany.

(*Received July* 3, 2003; *accepted in revised form May* 25, 2004).

Abstract—Far-from-equilibrium dissolution rates of a suite of volcanic glasses that range from basaltic to rhyolitic in composition were measured in mixed flow reactors at pH 4 and 10.6, and temperatures from 25 to 74°C. Experiments performed on glasses of similar composition suggest that dissolution rates are more closely proportional to geometric surface areas than their BET surface areas. Measured geometric surface area normalized dissolution rates ($r_{+,geo}$) at 25°C were found to vary exponentially with the silica content of the glasses. For pH 4 solutions this relation is given by:

$$\log r_{+,geo}(\mathrm{mol/m^2/s}) = -0.03 \cdot [\mathrm{SiO_2(wt\%)}] - 7.58, \quad \text{(A1)}$$

and at pH 10.6 ± 0.2 this relation is given by:

$$\log r_{+,geo}(\mathrm{mol/m^2/s}) = -0.02 \cdot [\mathrm{SiO_2(wt\%)}] - 7.02. \quad \text{(A2)}$$

These equations can be used to estimate lifetimes and metal release fluxes of natural glasses at far-from-equilibrium conditions. The lifetime at pH 4 and 25°C of a 1 mm basaltic glass sphere is calculated to be 500 yr, whereas that of a 1 mm rhyolitic glass sphere is 4500 yr. Estimated nutrient release rates from natural glasses decrease exponentially with increasing silica content.

1. INTRODUCTION

The influence of volcanic glass dissolution in natural processes cannot be overstated. Rapid cooling of magma on the Earth produces approximately one billion cubic meters (1 km^3) of glass each year, mainly along the 70000 km oceanic ridge system (Morgan and Spera, 2001). Most of this glass is of basaltic composition. According to Nesbitt and Young (1984), volcanic glass makes up ~12% of the average exposed continental crust surface, being surpassed in abundance only by plagioclase (~35%) and quartz (~20%). Dispersal of airborne volcanic glass "tephra," which follows explosive volcanic eruptions, primarily of high silicic composition, is an important part of the sedimentary processes in the North Atlantic (Haflidason et al., 2000; Larsen et al., 2001; Lacasse and Bogaard, 2002). Glass shards (>100 μm) fall on land and on the seafloor within a few hours or days after an explosive eruption (Carey, 1997). However, if highly vesicular pumice is produced, it can float for days or even years and consequently influence the chemistry of the ocean surface. Furthermore, glass of various compositions is one of the most important constituents of andisols, the main soil type present in volcanic terrains (Shoji et al., 1993). Owing to its abundance and rapid mechanical and chemical weathering, glass plays an important role in the global and local cycling of numerous elements and chemical species at the Earth's surface. Furthermore, sea floor weathering of submarine basaltic rocks and their glassy rims influences the long term CO_2 content of the atmosphere and therefore climate (Thompson, 1983; Alt et al., 1986; Staudigel et al., 1989; Brady, 1991; Francois and Walker, 1992; Spivack and Staudigel, 1994; Caldeira, 1995; Brady and Gislason, 1997; Alt and Teagle, 1999). Dissolution and secondary phase precipitation during weathering alter the chemistry of solutions in contact with glass and affect the chemical composition of rivers, lakes, and soils (White et al., 1980; Gislason and Eugster 1987b; Gislason et al., 1996; Kump et al., 2000; Chadwick and Chorover 2001). Moreover, basaltic glass is considered a natural analog for nuclear waste glasses (cf. Ewing and Haaker, 1979; Byers et al., 1985; Lutze et al., 1985). To model the long-term behaviour and stability of this radioactive waste confinement host studies have concentrated on laboratory corroded basaltic and synthetic borosilicate glasses and naturally altered basaltic glasses (Furnes, 1975, 1978; Seyfried Jr. and Bischoff, 1979; Allen, 1982; Malow et al., 1984; Crovisier et al., 1983, 1985, 1987, 1989a, 1989b; Grambow, 1985; Grambow et al., 1985; Berger et al., 1987, 1988, 1994; Gislason and Eugster, 1987a; Eggleton et al., 1987; Guy and Schott, 1989; Murukami et al., 1989; Jercinovic et al., 1990a, 1990b; Advocat et al., 1990, 1991, 1998; Nesbitt and Wilson, 1992; Ghiara et al., 1993; Gislason et al., 1993; Morgenstein and Shettel, 1994; Daux et al., 1994, 1997; Leturcq et al., 1999; Abraitis et al., 2000; Techer et al., 2001). Most of the natural glass dissolution studies were performed in either high ionic strength/seawater solutions or at high temperatures, and many were carried out in closed system batch reactors. These conditions promote the formation of secondary phases, which renders it difficult to unequivocally determine individual dissolution rates of the dissolving glass. To overcome this limitation, researchers have executed far-from-equilibrium dissolution rate studies in mixed

* Author to whom correspondence should be addressed (dwolff-boenisch@ucmerced.edu).

tapraid2/gca-gca/gca-gca/gca02204/gca3986d04z | xppws | S=1 | 9/16/04 | 15:00 | Art: W#2243 | DTD5.0

flow reactors in an attempt to unravel the underlying dissolution mechanism (e.g., Oelkers and Gislason, 2001; Gislason and Oelkers, 2003).

In contrast to the plethora of studies focussed on the dissolution rates of basaltic and borosilicate glasses, corresponding studies covering acidic volcanic glasses are less abundant. Studies of acid volcanic glass dissolution behaviour include work aimed at their potential utility as nuclear waste hosts (Kharkansis et al., 1980; Dickin, 1981; Petit, 1992 and references cited therein). Other studies centre on the leaching behaviour of silica rich glasses in an effort to better understand their dissolution mechanism (White and Claassen, 1980; White et al., 1980; White, 1983; Allnatt et al., 1983; Dran et al., 1986, 1988; Magonthier et al., 1992; Mungall and Martin, 1994; Mazer and Walther, 1994; Fiore et al., 1999). Another general objective of glass dissolution studies has been the extraction of leaching rates from natural systems like andisols (Shoji et al., 1993), andesitic to rhyolitic tephra/tuff/glass (Ruxton, 1988; Rowe and Brantley, 1993; Silber et al., 1999; Dahlgren et al., 1999) and the comparison with laboratory dissolution experiments (Yokoyama and Banfield, 2002).

The aforementioned studies illuminate different aspects of natural glass weathering, including temperature, pH, bacteria, inhibitory-catalytic ion effects, aqueous transport, or the degree of disequilibrium on natural glass dissolution kinetics. The few studies that have covered both the corrosion behaviour of basic *and* acidic glasses have been performed at high temperatures, neutral pH, and in batch reactors (Jantzen and Plodinec, 1984; Malow et al., 1984; Petit et al., 1990; Plodinec and Wicks, 1994).

Despite the impressive number of studies aimed at characterising the rates of natural glass dissolution, no simple correlation has been generated to describe the variation of far-from-equilibrium natural glass dissolution rates as a function of glass composition at the low temperatures typical of Earth surface environments. The objective of this study is to generate a correlation to quantify the role of natural glass dissolution in near surface processes. Towards this goal a suite of 18 chemically distinct glasses ranging from basaltic to rhyolitic was dissolved in mixed flow reactors. These results were used to generate simple equations describing natural glass far-from-equilibrium dissolution rates as a function of their chemical composition at low and high pH. These equations were employed to estimate lifetimes of volcanic glasses in soils. The results also facilitate the geochemical modelling of the nutrient release of Ca, Mg, K, and P under stoichiometric conditions from volcanic terrains, where tephra and pyroclastic material play a major role in soil formation. The purpose of this paper is to present the results of this experimental study and its implications for natural processes.

2. THEORETICAL BACKGROUND

All aqueous activities in the present study were generated using the PHREEQC 2.6 computer code (Parkhurst and Appelo, 1999). The only significant Al-bearing aqueous species considered in the thermodynamic model are Al^{3+}, $Al(OH)^{2+}$, $Al(OH)_2^+$, $Al(OH)_3^0$, and $Al(OH)_4^-$. Equilibrium constants were taken from the PHREEQC database for all aqueous species and minerals; these values were used to calculate hydrated volcanic glass equilibrium constants (K_{HVG}). According to Daux et al. (1997), Oelkers and Gislason (2001), and Gislason and Oelkers (2003), equilibrium constants for the dissolution of volcanic glasses can be estimated assuming that non-framework cations are leached out of the glass leaving a hydrated surface gel enriched in network forming cations. It is this gel that undergoes eventual hydrolysis. Therefore the K_{HVG} values refer to the hydrolysis reaction of this leached gel and not of the whole original glass, which does not attain thermodynamical equilibrium with the solution. The gel chemical formula consists of the glass network formers (Si and Al) and OH groups. Although Fe^{III} is a network former, it has been omitted from the gel chemical formula for two reasons: 1) determination of its aqueous activity in the reactors requires the knowledge of the redox conditions which are unknown; 2) due to potential incorporation of ferric iron into a variety of sites in the glass structure, the actual quantity in tetrahedral sites is not known. As the highest glass Fe_2O_3 content in the present study is less than 10% that of Si, it seems unlikely that omission of ferric iron will influence significantly the chemical affinity calculations reported in this study. Consistent with the reactions given in Table 1, K_{HVG} values were estimated for each composition from the stoichiometrically weighted sum of the amorphous silica and $Al(OH)_3$ hydrolysis reactions, which are also provided in this table. T1

The overall dissolution rate of a mineral or glass may be influenced by numerous factors including 1) the aqueous transport of chemical species away from its surface (cf. Murphy et al., 1989); 2) the effect of reverse reaction at near to equilibrium conditions (cf. Oelkers et al., 1994); and 3) the far-from-equilibrium dissolution rate. The goal of this current study is to compare the far-from-equilibrium dissolution rates of natural glasses as a function of their chemical composition. Experimental conditions were chosen, therefore, to assure that all rates measured in the present study are surface reaction controlled and at far-from-equilibrium conditions.

Numerous theoretical and experimental studies have described the variation of glass dissolution rates as a function of chemical affinity using (Lasaga, 1981; Aagaard and Helgeson, 1982; Helgeson et al., 1984; Grambow, 1985; Bourcier et al., 1990; Berger et al. 1994; Daux et al., 1997):

$$\boldsymbol{r} = \boldsymbol{r}_{+}(1 - \exp(-\mathrm{A}^{*}/\sigma \boldsymbol{R}\boldsymbol{T})) \quad (1)$$

where $\boldsymbol{r}$ and $\boldsymbol{r}_{+}$ designate the overall and forward dissolution rate, respectively, $\boldsymbol{A}^*$ refers to the chemical affinity for the hydrolysis reaction of the hydrated leached surface gel, which differs from that of the bulk glass, $\boldsymbol{\sigma}$ stands for Temkin's average stoichiometric number equal to the ratio of the rate of destruction of the activated or precursor complex relative to the overall rate, $\boldsymbol{R}$ designates the gas constant, and $\boldsymbol{T}$ represents absolute temperature. Different approaches had been adopted to quantify $\boldsymbol{A}^*$. For example, Grambow (1985) and Berger et al. (1994) observed that the hydrated surface layer during their glass dissolution experiments consisted of an amorphous Si-rich layer and suggested that $\boldsymbol{A}^*$ can be assumed equal to the chemical affinity of amorphous silica. In contrast, Bourcier et al. 1990) and Daux et al. (1997) suggested that $\boldsymbol{A}^*$ can be assumed equal to the chemical affinity of an amorphous gel containing SiO_2 + $Al(OH)_3$ ± $Fe(OH)_3$, $Ca(OH)_2$ and

Table 1. The composition of the hydrated volcanic glasses (HVG), their hydrolysis reactions and the logarithm of the equilibrium constants (K_{HVG}) of these reactions used to estimate saturation indices.

Sample	Volcanic name	Hydrolysis reaction for the HVG under acid conditions	log K_{HVG}
BT	rhyolite	$SiAl_{0.20}O_2(OH)_{0.61} + 0.61H^+ + 1.39H_2O = H_4SiO_4 + 0.20Al^{3+}$	−0.55
Ö62	rhyolite	$SiAl_{0.22}O_2(OH)_{0.65} + 0.65H^+ + 1.35H_2O = H_4SiO_4 + 0.22Al^{3+}$	−0.33
HI	rhyolite	$SiAl_{0.23}O_2(OH)_{0.69} + 0.69H^+ + 1.31H_2O = H_4SiO_4 + 0.23Al^{3+}$	−0.23
H3W	rhyolite	$SiAl_{0.23}O_2(OH)_{0.70} + 0.70H^+ + 1.30H_2O = H_4SiO_4 + 0.23Al^{3+}$	−0.23
A75	rhyolite	$SiAl_{0.21}O_2(OH)_{0.63} + 0.63H^+ + 1.37H_2O = H_4SiO_4 + 0.21Al^{3+}$	−0.44
H3B	dacite	$SiAl_{0.26}O_2(OH)_{0.78} + 0.78H^+ + 1.22H_2O = H_4SiO_4 + 0.26Al^{3+}$	0.10
HZ0	dacite	$SiAl_{0.29}O_2(OH)_{0.86} + 0.86H^+ + 1.14H_2O = H_4SiO_4 + 0.29Al^{3+}$	0.42
SLN	dacite	$SiAl_{0.27}O_2(OH)_{0.81} + 0.81H^+ + 1.19H_2O = H_4SiO_4 + 0.27Al^{3+}$	0.21
H20	basaltic andesite	$SiAl_{0.31}O_2(OH)_{0.93} + 0.93H^+ + 1.07H_2O = H_4SiO_4 + 0.31Al^{3+}$	0.64
HZ1	basaltic andesite	$SiAl_{0.32}O_2(OH)_{0.97} + 0.97H^+ + 1.03H_2O = H_4SiO_4 + 0.32Al^{3+}$	0.75
HZ3	basalt	$SiAl_{0.33}O_2(OH)_{0.99} + 0.99H^+ + 1.01H_2O = H_4SiO_4 + 0.33Al^{3+}$	0.85
GR	basalt	$SiAl_{0.32}O_2(OH)_{0.95} + 0.95H^+ + 1.05H_2O = H_4SiO_4 + 0.32Al^{3+}$	0.75
HE1	mugearite	$SiAl_{0.38}O_2(OH)_{1.13} + 1.13H^+ + 0.87H_2O = H_4SiO_4 + 0.38Al^{3+}$	1.39
A61	basalt	$SiAl_{0.30}O_2(OH)_{0.90} + 0.90H^+ + 1.10H_2O = H_4SiO_4 + 0.30Al^{3+}$	0.53
KRA	basalt	$SiAl_{0.32}O_2(OH)_{0.96} + 0.96H^+ + 1.04H_2O = H_4SiO_4 + 0.32Al^{3+}$	0.75
KAT	basalt	$SiAl_{0.32}O_2(OH)_{0.95} + 0.95H^+ + 1.05H_2O = H_4SiO_4 + 0.32Al^{3+}$	0.75
SS	basalt	$SiAl_{0.42}O_2(OH)_{1.25} + 1.25H^+ + 0.75H_2O = H_4SiO_4 + 0.42Al^{3+}$	1.83
ELD	basalt	$SiAl_{0.33}O_2(OH)_{1.00} + 1.00H^+ + 1.00H_2O = H_4SiO_4 + 0.33Al^{3+}$	0.85

Example of the calculation of ELD's K_{HVG}: (amorphous) $SiO_2 + 2\ H_2O = H_4SiO_4$; log K −2.71 (PHREEQC) (amorphous) $Al(OH)_3 + 3\ H^+ = Al^{3+} + 3\ H_2O$; log K 10.80 (PHREEQC) $1(Si) \cdot -2.71 + 0.33(Al) \cdot 10.80 = 0.85$.

$Mg(OH)_2$. Each of these studies accurately described various glass dissolution data sets as a function of solution composition at near to equilibrium conditions.

The present study is focused on glass dissolution rates at far-from-equilibrium conditions. This makes it possible to determine the effect of glass composition on the dissolution rates, independently of those stemming from the reverse reaction (e.g., re-precipitation of the leached surface gel). The form of Eqn. 1 is such that overall rates $\boldsymbol{r}$ equal forward rates $\boldsymbol{r}_+$ when $\boldsymbol{A^* >> \sigma RT}$. Note that although Eqn. 1 has not yet been proven to describe the dissolution rates of all glasses, it has provided accurate descriptions of the dissolution rates of a variety of glasses (Grambow, 1985; Bourcier et al., 1990; Berger et al., 1994; Daux et al., 1997), as well as quartz (Berger et al., 1994), feldspars (Oelkers et al., 1994; Gautier et al., 1994) and halite (Alkattan et al., 1997). According to Eqn. 1, as one approaches equilibrium, overall rates $\boldsymbol{r}$ decrease systematically and are equal to zero at equilibrium with the surface, where $\boldsymbol{A^* = 0}$; $\boldsymbol{r}$ is within 10% of $\boldsymbol{r}_+$ when $\boldsymbol{A^*/\sigma RT > 2.3}$. All dissolution rates measured in the present study were performed at conditions where $\boldsymbol{A^*/RT > 6.5}$, where in this case $\boldsymbol{A^*}$ refers to the chemical affinity of the hydrated glasses in accord with the reactions in Table 1.

An additional complicating factor in deducing the effect of natural glass composition on far-from-equilibrium dissolution rates is that these rates may also depend on aqueous solution composition. Basaltic glass dissolution rates were found to vary with aqueous solution composition in accord with (Oelkers, 2001; Oelkers and Gislason, 2001; Gislason and Oelkers, 2003):

$$\boldsymbol{r}_+ = \boldsymbol{ks}\left(\frac{\boldsymbol{a}^3_{H^+}}{\boldsymbol{a}_{Al^{3+}}}\right)^{1/3} \quad (2)$$

where $\boldsymbol{k}$ denotes a rate constant, $\boldsymbol{s}$ stands for the surface area, and $\boldsymbol{a}_i$ designates the aqueous activity of the subscripted species. Eqn. 2 suggests that constant pH far-from-equilibrium basaltic glass dissolution rates will be independent of aqueous Si activity, but decrease with aqueous Al activity (e.g., increasing aqueous Al concentration or decreasing aqueous Al complex formation). Basaltic glass dissolution rates as a function of aqueous Si, Al, and organic acid concentration were found to closely correspond to those computed using Eqn. 2 (Oelkers and Gislason, 2001). To allow comparison of natural glass dissolution rates as a function of their chemical composition independent of potential effects of solution composition, the $(\boldsymbol{a}^3_{H^+}/\boldsymbol{a}^{3+}_{Al})$ activity ratio was kept approximately constant in all experiments. Log $(\boldsymbol{a}^3_{H^+}/\boldsymbol{a}^{3+}_{Al})$ for the 25°C experiments was fixed at -6.4 ± 0.6. This ± 0.6 log variation leads to a corresponding variation on rates in Eqn. 2 of ± 0.2 log units.

3. MATERIAL AND METHODS

3.1. Materials and Sample Preparation

Seventeen volcanic glasses from Icelandic volcanic eruptions of the last 3200 yr were selected for this study. One specimen comes from an ignimbrite pyroclastic flow of the Bishop Tuff complex, Long Valley, California (Hildreth, 1979) and was added to this study to enlarge the glass composition range. The chemical compositions of these 18 specimens were determined by XRF with a Philips PW-1404 spectrometer and are shown in Table 2. Only glass specimens that appeared macroscopically "fresh," i.e., without any alteration features, were sampled but potential weathering of the tephra and pumices on a microscopic scale cannot be ruled out. Glass specimens were either taken directly from the scoria part of lava flows near the eruption craters or from tephra (ash) fallout deposits. In the latter case, to minimise the effect of aging, the volcanic ashes were sampled close to the source, where the "grains" are of maximum size and the ash layers of maximum thickness (up to several meters in thickness). For the rhyolitic glasses the diameter of the pumice ranged from several centimetres to tens of centimetres. These glasses were dried, first at ambient temperature in the laboratory and then at 50°C for several days. The samples were subsequently brushed and shaken to remove adhered particles. The glass KRA was treated with hydrogen peroxide before grinding to remove lichen and plant roots. All samples were ground in plastic bags using a plastic hammer in an attempt to induce minimum strain to the fresh surfaces. Subsequent dry sieving yielded the 45–125 μm size fraction. This fraction was ultrasonically cleaned, first in deionised

tapraid2/gca-gca/gca-gca/gca02204/gca3986d04z | xppws | S=1 | 9/16/04 | 15:00 | Art: W#2243 | DTD5.0

Table 2. XRF chemical analyses of the volcanic glasses in weight percent. Major element reproducibility yielded relative standard deviations <2% for all the oxides.

Sample*	Code	SiO_2	TiO_2	Al_2O_3	Fe_2O_3	FeO	MnO	MgO	CaO	Na_2O	K_2O	P_2O_5	LO1
Bishop Tuff, 0.76 Ma[#]	BT	72.62	0.08	12.48	0.78	0.11	0.03	0.09	0.48	3.79	4.38	0.01	4.83
Öraefajökull 1362	Ö62	70.64	0.24	13.00	2.40	1.18	0.10	0.02	0.97	5.45	3.41	0.02	1.95
Hekla 1104	H1	70.59	0.22	13.78	1.10	2.28	0.11	0.09	1.92	4.88	2.67	0.04	1.40
Hekla 3W, 2900 BP	H3W	69.79	0.21	13.79	1.15	2.32	0.11	0.11	2.08	4.83	2.48	0.04	1.90
Askja 1875	A75	69.28	0.90	12.42	2.48	2.09	0.10	0.97	2.81	3.74	2.21	0.19	1.70
Hekla 3B, 2900 BP	H3B	66.01	0.42	14.65	2.14	3.81	0.18	0.39	3.21	4.72	2.07	0.10	0.97
Hekla Z0, 2300 BP	HZ0	62.80	0.96	15.34	2.64	4.53	0.17	1.40	4.57	4.35	1.55	0.34	0.20
Silk-LN, 3100 BP	SLN	62.76	1.26	14.36	2.09	4.15	0.19	1.05	2.94	4.62	2.55	0.30	2.64
Hekla 2000[†]	H20	54.81	1.98	14.35	4.38	7.48	0.27	2.81	6.65	4.01	1.27	0.96	−0.43
Hekla Z1, 2300 BP	HZ1	54.14	2.00	14.81	6.31	5.55	0.26	2.93	6.53	3.66	1.20	1.01	0.20
Hekla Z3, 2300 BP	HZ3	51.62	2.36	14.49	6.00	7.11	0.28	3.30	6.96	3.29	1.06	1.27	0.57
Grimsvötn 1998[†]	GR	50.77	2.53	13.55	2.57	10.26	0.20	5.54	9.87	2.77	0.52	0.28	−0.93
Heimaey 1973[†]	HEI	50.48	2.24	16.16	3.78	7.77	0.25	2.54	6.94	5.84	1.60	0.78	−0.23
Askja 1961	A61	50.13	2.73	12.74	4.91	10.73	0.24	4.66	8.97	2.70	0.56	0.31	−0.70
Krafla 1984	KRA	49.78	2.01	13.44	3.06	11.56	0.23	5.73	10.23	2.37	0.32	0.20	−0.87
Katla 1755	KAT	47.07	4.50	12.65	4.13	11.08	0.23	4.79	9.11	2.79	0.77	0.64	0.00
Surtsey 1964[†]	SS	46.48	2.46	16.35	2.57	9.66	0.19	5.88	9.87	3.60	0.67	0.33	−0.13
Eldgjá 934	ELD	46.09	4.35	12.98	6.11	9.65	0.21	5.31	10.15	2.59	0.66	0.44	−0.26

[#] van den Bogaard and Schirnick. 1995.

* Sample names consist of the sample location and eruption date. 0.76 Ma refers to 0.76 million years before present, 2900 BP stands for 2900 years before present, and 1104 represents the year 1104. Exact dates of eruptions occuring before 934 are somewhat uncertain.

[†] Specimens from these eruptions were taken days to weeks after the volcanic activity, i.e. eruption age does not equal weathering age.

water, and then in acetone, by separating and discarding the ultra fine suspension at the end of each cleaning cycle, which lasted for 10 min. Altogether five water and acetone cycles were carried out to remove fine particles. The particle size distribution is assumed to be identical for all glasses. Finally, the powders were dried overnight at 110°C. The specific surface area of the glasses before the dissolution experiments was measured by the three-point BET method using Kr gas.

3.2. Experimental Methods

Dissolution experiments were performed in two different mixed-flow reactors. One reactor system consists of a 300 mL Parr™ titanium mixed flow reactor equipped with a stirring and temperature controller (cf. Dove and Crerar, 1990). The solution was pumped through the reactor at a constant rate of 0.9 to 3.0 mL/min using a High Pressure Liquid Chromatography (HPLC) pump. To ensure that aqueous transport away from the solid-solution interface did not affect glass dissolution kinetics, the stirring rate was set to 350 rpm. Gislason and Oelkers (2003) demonstrated that at a rotation speed of 325 rpm, basaltic glass dissolution at pH 3.3 in this reactor system is surface reaction controlled. As the dissolution rates measured in this study were performed at higher pH and on glasses which in general have higher silica contents, these rates are slower than the basaltic glass dissolution rates measured by Gislason and Oelkers (2003). It seems therefore reasonable to assume that aqueous transport away from the solid-solution interface does not affect glass dissolution kinetics in the present study. The second reactor system was composed of acid washed PE™ 300 mL reactors maintained at constant temperature in a thermostat controlled water bath. These reactors were stirred using Teflon™ coated floating stir bars from Nalgene™ placed on the bottom of the reactors and propelled by a multi-position magnetic stirrer located underneath the water bath. Pumping rates from 0.7–3.0 mL/min were maintained using a Masterflex™ cartridge pump. Experiments performed in both reactors on the same glass powder, and at the same temperature and flow rate, yielded identical results. This observation demonstrates the consistency of experiments performed in these two different reactor systems. Although the stirring of mixed flow reactors may lead to increasing surface areas during dissolution experiments (Metz and Ganor, 2001), the observation that steady state conditions lasted for up to four weeks suggests this effect was not significant in the present study (see Fig. 1). In the present study the BET surface area of the specimens was not determined after the dissolution experiments.

All experiments were performed at pH 4 or 10.6 and ionic strength of 10 mM. Acid inlet solutions comprised Millipore™ water and Merck analytical grade NH_4Cl and HCl; alkaline solutions comprised Millipore™ water and Merck analytical grade NH_4Cl and NH_3. The compositions of these inlet solutions were computed using the PHREEQC-2 program to yield the desired pH and ionic strength. The concentrations of cations released during the experiments were 5% or less than the ionic strength of the inlet solutions. Thus the ionic strength remains essentially constant throughout the experiments. No Si was detected in the inlet solutions.

Inlet solutions with alkaline pH were continuously purged with N_2 during the experiments to prevent dissolved carbonate precipitation due to CO_2 entering the reactor. At the beginning of each experimental series the reactor was thoroughly cleaned, assembled, and run for 24 h with a 0.1 mol/L hydrochloric solution to rinse the tubing and clean the reactor. The reactor was then flushed with deionised water. Between 1 and 8 g of dry glass powder were put in the reactor. The reactor was then filled with the inlet solution, closed tightly, and placed in the water bath or furnace jacket (in the case of the Parr™ reactor). Flow, temperature, and stirring rates were adjusted to desired settings. The outlet flow was sampled, filtered through a 0.2 μm cellulose acetate filter, acidified with concentrated supra-pure HNO_3, and analysed for the silica content. Outlet silica content was monitored using the molybdenum blue method (Fishman and Friedman, 1989). When the silica concentrations reached steady state, the experiment was either stopped or the temperature and/or the fluid flow rate were adjusted to a new setting. Following the experiments, Si, Al, Na, Mg, Ca, and Fe concentration of the outlet solutions were determined by ICP-AES. Species distribution calculations performed using PHREEQC 2.6 indicate that all pH 4 outlet solutions were undersaturated with respect to all potential secondary phases. The pH 10.6 outlet solutions were undersaturated with respect to all silicate minerals, but supersaturated with respect to hematite, goethite, and amorphous iron-hydroxide.

Samples of the glass, before and after the experiments, were studied by Scanning Electron Microscopy (SEM). Specimens were mounted on glass slides, subsequently carbon coated and observed in a JEOL JSM 6300F at 20kV and imaged using analySIS imaging software. The samples were carefully examined at low (×100) and high (×30000) magnification for surface features before and after dissolution experiments. Energy Dispersive X-ray (EDX) analyses were made using an Oxford Instrument OX 2000 INCA system and the spectra compared for changes in element composition. Some of the samples were also

tapraid2/gca-gca/gca-gca/gca02204/gca3986d04z | xppws | S=1 | 9/16/04 | 15:00 | Art: W#2243 | DTD5.0

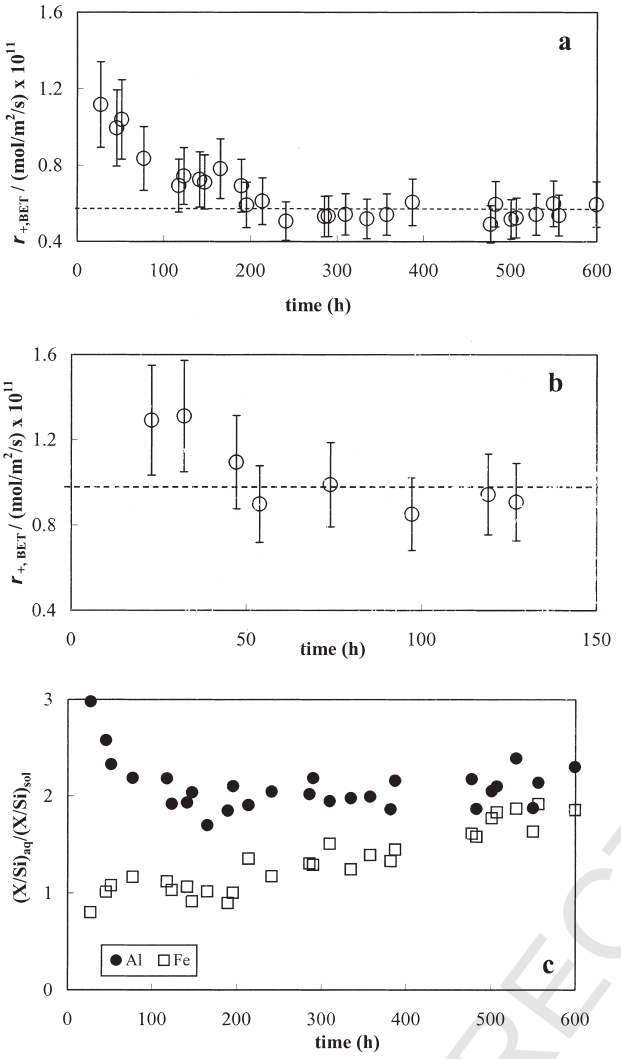

Fig. 1. (a) Temporal variation of the BET normalized dissolution rate of the basalt ELD versus time, (b) Temporal variation of the BET normalized dissolution rate of the rhyolite H1 versus time, (c) $(X/Si)_{aq}/(X/Si)_{glass}$ ratio of the dissolution of ELD with time, X = Al, Fe.

embedded in epoxy resin and sectioned to look for any dissolution or replacement changes in cross-section at or near the outside edges of the sample grains.

4. RESULTS

4.1. Steady State Dissolution Rates

Far-from-equilibrium steady state dissolution rates ($r_{+,i}$) are calculated using:

$$r_{+,i} = \frac{C_{Si} \cdot fr}{A_i \cdot m} \quad (3)$$

where C_{Si} designates the aqueous Si concentration of the outlet solution, fr represents the fluid flow rate, A_i is the specific surface area of the dissolving glass, m the mass of sample, and the index (i) corresponds to the method used to define the specific surface area. Dissolution rates in the present study have been normalized to either measured BET specific surface areas or the computed geometric specific surface areas of the dissolving glass powders. The geometric specific surface area A_{geo} is calculated by (Brantley et al., 1999; Gautier et al., 2001):

$$A_{geo} = \frac{6}{\rho \cdot d_{eff}} \quad (4)$$

where ρ is the glass density and d_{eff} is the effective particle diameter. The number 6 is based on the assumption that grains have a regular and smooth spherical shape. Assuming a homogeneous particle distribution, d_{eff} can be obtained from (Tester et al., 1994):

$$d_{eff} = \frac{d_{max} - d_{min}}{\ln\left(\frac{d_{max}}{d_{min}}\right)} \quad (5)$$

where d_{max} and d_{min} refer to the maximum and minimum particle size of the size fraction used in the experiments. The ratio between BET and geometric surface area (A_{BET}/A_{geo}) is commonly denominated surface roughness. This use of the term surface roughness is, however, inconsistent with the definition of Jaycock and Parfitt (1981), who defined surface roughness as the average peak-to-trough *height* of surface features measured to a reference surface plane. To avoid confusion with the Jaycock and Parfitt (1981) definition, the (A_{BET}/A_{geo}) ratio will be referred to in the present study by the term roughness factor. Both surface areas, roughness factors, calculated glass densities (ρ), and glass sample masses used in the experiments are compiled in Table 3. The particle densities of the volcanic glasses were computed using the software program KWare Magma (Wohletz, 2002). This program calculates rock/glass densities by the method of Bottinga and Weil (1972). Note that the particle density signifies maximum density, without pore space, so it does not include provision for vesicularity. Although the glasses were ground to 45–125 μm, many specimens still display some porosity (Fig. 2). Because a) not all glasses display vesicularity, b) not all glass particles display the same vesicularity, and c) not all pores have the same size, it is not possible to estimate the porosity of the glass powders used in the present study. Consequently, the maximum densities generated by KWare Magma are reported and used in the present study. Uncertainties associated with adopting this assumption are discussed below.

All experimentally measured steady state dissolution rates are listed in Tables 4 and 5. Steady state dissolution rates, normalized to both BET and geometric surface area are provided in these tables. As the roughness factor is generally greater than 1, dissolution rates normalized to the BET surface area ($r_{+,BET}$), are smaller than those normalized to geometric surface areas ($r_{+,geo}$). Dissolution rates in the present study are based on Si release rates. Steady state dissolution is assumed when the outlet Si concentration is constant within analytical uncertainty for more than three residence times. The residence time of the reactor is defined as the volume of the reactor divided by the fluid flow rate. Note that network modifying cations may still exhibit non-steady state release rates after Si steady state has been attained. Two examples of the attainment of steady state are illustrated in Figures 1a and b. The figures present silicon outlet solution concentrations during the dissolution of the basaltic glass ELD and the rhyolitic glass

tapraid2/gca-gca/gca-gca/gca02204/gca3986d04z | xppws | S=1 | 9/16/04 | 15:00 | Art: W#2243 | DTD5.0

Table 3. Summary of physical properties of the glass powders used in this study. Determined apparent activation energies E_a are included.

Sample	Volcanic name	Glass density* g/cm^3	A_{BET} cm^2/g/10^4	A_{geo} cm^2/g	Roughness factor	E_a kJ/mol pH 4	E_a kJ/mol pH 10.6
BT	rhyolite	2.31	3.12	332	94	41.7	—
Ö62	rhyolite	2.36	0.43	324	13	35.5	—
H1	rhyolite	2.42	0.56	317	18	31.7	—
H3W	rhyolite	2.42	1.08	316	34	38.1	52.6
A75	rhyolite	2.45	1.41	312	45	31.8	51.8
H3B	dacite	2.51	1.21	305	40	38.1	55.6
HZ0	dacite	2.59	0.62	296	21	—	—
SLN	dacite	2.55	2.65	301	88	—	—
H20	b-andesite	2.79	0.12	275	4	—	—
HZ1	b-andesite	2.73	2.16	280	77	—	—
HZ3	basalt	2.81	4.34	273	159	—	—
GR	basalt	2.99	0.11	256	4	—	—
HEI	mugearite	2.81	0.07	272	3	43.3	49.9
A61	basalt	2.99	0.14	256	6	—	—
KRA	basalt	3.04	0.14	252	6	27.2	41.3
KAT	basalt	3.04	0.94	252	37	—	—
SS	basalt	3.00	0.19	255	8	—	—
ELD	basalt	3.02	5.22	253	206	—	—

* Corresponds to the particle density, not corrected for potential vesicularity, see text "b-" means basaltic.

H1, respectively, in pH 4 solutions at 25°C. The residence times for these experiments were 5 h each. If the metal release rates from the glasses were constant, then a fluid dynamic steady state would be achieved after ~3–4 residence times, i.e., after 15–20 h. Partially detached silica tetrahedra, which are bonded to the glass surface by only one or two bridging oxygens, are abundant on the original glass powders, mainly at edges and sharp tips. The dissolution rate of such Si is relatively fast and thus the silica concentration in the outlet fluid is relatively high at the onset of the experiments (Oelkers and Gislason, 2001; Gislason and Oelkers, 2003). With time, these high surface energy sites disappear as tips and edges get rounded off (cf. Figs. 2g, h) and dissolution slows such that the Si release rate eventually becomes constant. In the case of the rhyolite H1, steady state is reached after 50 h. Oelkers and Gislason (2001) and Gislason and Oelkers (2003) found steady state for basaltic glasses to occur after less than a day. In contrast, the basaltic glass ELD took as much as 200 h to reach steady state (cf. Fig. 1a); this may be due to the presence of an iron coating on its surface.

The temporal variation in the aluminium/silicon and iron/silicon concentration ratio of the outlet fluid during the dissolution of glass ELD normalized to that of the dissolving glass is shown in Figure 1c. Al is released preferentially to silicon at the onset of the experiment, but with increasing time and glass dissolution, this ratio diminishes to a constant value. In contrast, Fe dissolves congruently at the beginning of the experiment, but the aqueous Fe/Si ratio rises slowly with elapsed time. This behaviour likely stems from the dissolution of the above mentioned iron phases on the glass surface rather than due to the precipitation of an Al/Si rich phase during dissolution. Solute speciation calculations indicate that the pH 4 reactive solution is undersaturated with respect to all common Al and Si bearing phases (e.g., amorphous SiO_2, amorphous $Al(OH)_3$, quartz, gibbsite, and kaolinite). This interpretation is also supported by the fact that these pH 4 solutions are undersaturated with respect to iron (oxy)hydroxide phases. In contrast, at pH 10.6, iron (oxy)hydroxide phases are supersaturated and the outlet solutions are strongly depleted in aqueous Fe consistent with iron (oxy)hydroxide precipitation. Nevertheless, the outlet Si concentration in these pH 10.6 experiments attains and maintains a steady state concentration, suggesting that the presence of iron precipitates does not affect Si release. $(Al/Si)_{aq}/(Al/Si)_{glass}$ ratios at steady state of all experiments are listed in Tables 4 and 5. These $(Al/Si)_{aq}/(Al/Si)_{glass}$ values generally range from 0.3 to 3 indicating that the outlet fluid stoichiometry is consistent within a factor of 3 to that of the dissolving glass. Steady state $(Al/Si)_{aq}/(Al/Si)_{glass}$ values are generally greater than 1 suggesting leached layer formation.

Dissolution rates at elevated temperatures were used to estimate apparent activation energies (E_a) calculated for some of the glasses (Table 3). Apparent activation energies were generated using:

$$E_a = -\frac{\partial \ln r_{+,geo}}{\partial (1/T)} \cdot R \qquad (6)$$

The calculated E_a values range from 24 to 43 kJ/mol for basaltic and 32 to 42 kJ/mol for acidic glasses at pH 4; E_a values are somewhat higher at pH 10.6. Variation is evident among the E_a values in Table 3. The reason for this variation is likely the small temperature range for which E_a values were determined; such a small temperature range magnifies both small experimental uncertainties and potential effects of aqueous solution composition on computed E_a values.

4.2. SEM

SEM images of some "fresh" glasses (before experiments) described in Table 2 are shown in Figure 2a to f. The first two images, 2a and b, are from the basalts HEI and SS. HEI reveals a smooth bubble-free surface, which is consistent with its low roughness factor of 3, as listed in Table 3. Similarly, the smooth surfaces of SS are consistent with its low roughness factor of 8. The SEM images, c and d, depict the surfaces of the andesitic

tapraid2/gca-gca/gca-gca/gca02204/gca3986d04z | xppws | S=1 | 9/16/04 | 15:00 | Art: W#2243 | DTD5.0

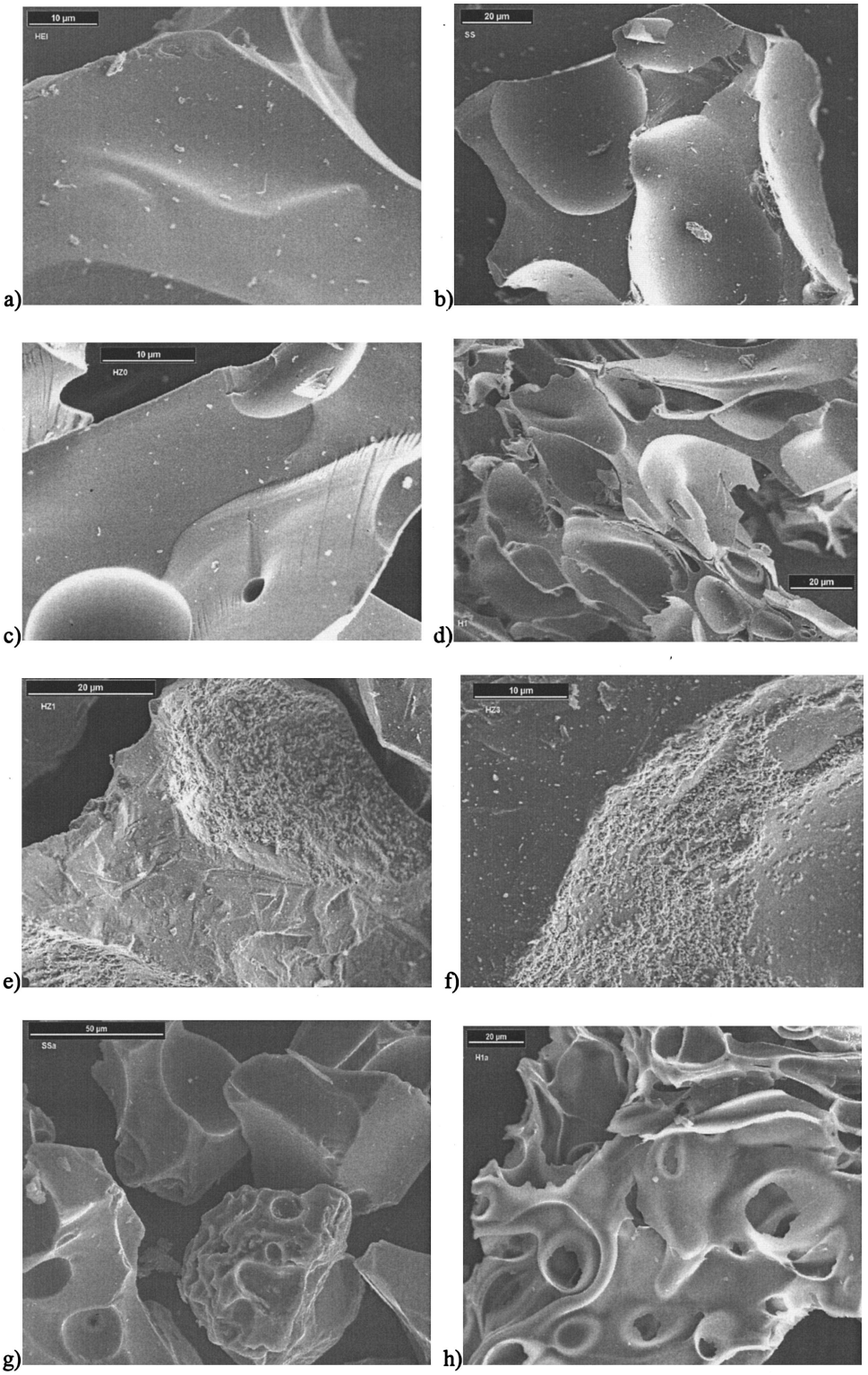

Fig. 2. SEM photos of selected volcanic glass powders. a) HEI (A_{BET}: 0.07 m^2/g) before dissolution, b) SS (A_{BET}: 0.19 m^2/g) before dissolution, c) HZ0 (A_{BET}: 0.62 m^2/g) before dissolution, d) H1 (A_{BET}: 0.56 m^2/g) before dissolution, e) HZ1 (A_{BET}: 2.16 m^2/g) before dissolution, f) HZ3 (A_{BET}: 4.34 m^2/g) before dissolution, g) SS post dissolution at pH 4, h) H1 post dissolution at pH 4.

tapraid2/gca-gca/gca-gca/gca02204/gca3986d04z | xppws | S=1 | 9/16/04 | 15:00 | Art: W#2243 | DTD5.0

Table 4. Experimental results of the dissolution rate experiments at acidic pH. The glasses are ordered from high to low silica content

Sample	temp. °C	Mass g	pH	Flow rate g/min	Si μmol/l	Al μmol/l	Al/Si[#]	A^* kJ/mol	log (a_H^{3+}/a_{Al}^{3+})	log $r_{+\ BET}$ mol/m^2/s	log $r_{+\ geo}$ mol/m^2/s
BT-3	25	8.00	4.20	0.96	4.71	2.01	0.9	19.9	−6.5	−11.52	−9.55
BTF-3	25	7.00	4.11	0.83	4.34	3.30	3.8	19.5	−6.5	−11.53	−9.56
Ö62-5	25	7.50	4.05	1.04	1.92	1.20	2.9	23.3	−5.8	−10.99	−9.87
Ö62F-4	25	8.01	4.11	0.93	2.34	2.32	4.6	23.0	−6.3	−10.98	−9.85
HI-8	25	7.50	4.00	1.09	2.10	1.32	2.7	23.5	−5.8	−11.04	−9.80
H3W-4	25	4.50	4.13	1.00	2.83	3.88	5.9	21.8	−6.6	−11.01	−9.48
H3WF-1	25	4.80	4.03	0.87	2.91	3.19	4.7	20.9	−6.2	−11.09	−9.55
A75-8	25	7.50	4.07	1.09	3.24	1.84	2.7	21.5	−6.1	−11.25	−9.60
A75F-1	25	7.61	4.15	0.87	6.23	2.81	2.1	21.7	−6.5	−11.09	−9.43
H3B-4	25	4.00	4.02	1.06	3.29	1.61	0.8	23.2	−5.9	−10.72	−9.12
HZ0-5	25	4.95	4.04	0.97	2.68	2.19	2.8	24.1	−6.1	−10.86	−9.53
SLN-2	25	5.00	4.06	0.96	4.82	4.37	3.4	24.4	−6.4	−11.23	−9.29
SLNF-3	25	5.02	4.12	1.26	6.61	6.71	3.8	21.6	−6.8	−10.98	−9.04
H20-2	25	3.01	4.11	1.14	1.64	1.26	2.5	21.5	−6.0	−10.06	−9.42
HZ1-6	25	3.00	4.03	0.92	5.35	3.48	2.0	26.0	−6.2	−10.90	−9.01
GR-6	25	1.90	4.07	0.90	2.08	1.62	2.5	23.0	−6.0	−9.83	−9.19
HE1-5	25	3.04	4.16	0.95	5.31	3.28	1.6	25.5	−6.6	−9.41	−8.99
HEIF-2	25	3.00	4.00	1.26	4.14	2.05	1.3	23.7	−5.9	−9.39	−8.97
A61-5	25	1.75	4.08	0.93	2.24	1.34	2.0	23.5	−6.0	−9.86	−9.11
KRA-6	25	3.04	4.12	0.95	4.60	2.71	1.9	25.1	−6.4	−9.77	−9.02
KAT-6	25	1.42	4.17	0.96	3.59	2.55	2.2	23.0	−6.5	−10.37	−8.80
SS-5	25	1.32	4.17	0.92	2.46	1.72	1.7	23.4	−6.3	−9.83	−8.95
SSF-4	25	2.50	4.17	0.98	5.87	4.25	1.7	27.1	−6.7	−9.71	−8.82
ELD-20	25	2.00	4.00	0.92	4.14	2.97	2.2	27.2	−6.1	−11.22	−8.90
HEI-15	30	3.00	4.09	1.19	6.17	2.45	1.1	24.4	−6.3	−9.25	−8.83
KRA-9	32	3.04	4.06	1.32	3.54	1.24	1.1	25.2	−5.9	−9.74	−8.99
H1-13	35	7.50	4.02	1.56	2.49	1.36	2.4	23.9	−5.8	−10.81	−9.57
H3B-7	37	4.00	3.99	1.44	2.20	1.29	1.0	25.5	−5.7	−10.76	−9.16
HEI-16	39	3.00	4.08	1.52	7.32	2.53	0.9	24.9	−6.2	−9.07	−8.65
KRA-17	40	3.04	4.08	1.26	5.56	2.20	1.2	24.1	−6.1	−9.56	−8.82
BT-8	40	8.00	4.05	1.37	6.16	0.96	0.3	21.2	−5.7	−11.25	−9.28
H3W-8	40	4.50	4.03	1.51	3.38	1.63	2.1	23.5	−5.9	−10.76	−9.22
A75-13	40	7.50	4.04	1.08	5.66	1.08	0.9	21.6	−5.7	−11.02	−9.36
H1-18	42	7.50	4.04	1.56	2.66	0.90	1.5	24.5	−5.6	−10.78	−9.54
Ö62-11	45	7.50	3.99	1.94	2.40	0.71	1.4	24.9	−5.3	−10.62	−9.50
H3B-13	50	4.00	4.01	1.65	3.64	2.12	1.0	25.0	−5.8	−10.48	−8.88
H1-32	50	7.50	4.04	2.20	3.06	0.61	0.9	25.1	−5.4	−10.57	−9.33
A75-16	52	7.50	4.16	1.08	10.28	1.34	0.6	20.5	−6.0	−10.76	−9.10
BT-13	55	8.00	4.03	1.49	13.70	2.42	0.4	19.8	−5.9	−10.87	−8.89
H3W-14	55	4.50	4.03	1.99	5.35	1.47	1.2	23.6	−5.7	−10.44	−8.90
H1-34	56	7.50	4.04	2.52	3.19	0.73	1.0	25.4	−5.4	−10.50	−9.25
Ö62-15	60	7.50	4.02	2.05	4.49	1.07	1.1	24.3	−5.4	−10.32	−9.20
A75-26	74	7.50	3.99	3.03	6.82	1.46	0.9	24.2	−5.2	−10.49	−8.83

[#] Molar $(Al/Si)_{aq}/(Al/Si)_{glass}$ ratio.

glass HZ0 and the rhyolite H1. Although the surfaces of these glasses are smooth and free of most fine particles, they exhibit rough surfaces due to the presence of bubbles leading to some porosity within the grains. Consequently the surface roughness of these glasses is relatively high; the roughness factors of HZ0 and H1 are 21 and 18, respectively. Figures 2e and f show SEM images of the basaltic andesite HZ1 and the basalt HZ3. These glasses exhibit some surface coatings. As a result, the roughness factors of HZ1 and HZ3 are 77 and 159, respectively. EDX analyses show these surface coatings to be iron nonsilicates. Similar observations were made on sample ELD, which has a roughness factor of 206. As these coatings will only contribute to surface area and may not affect Si release during dissolution experiments (Hodson, 2003), HZ1 and ELD are retained in the dissolution study described below. In contrast, SEM back scattering images of glass cross sections showed that HZ3 contained Si bearing mineral phases that could contribute to measured Si release. This sample was thus eliminated from this dissolution study.

Figures 2g and 2h show SEM images from the glasses SS and H1 after their dissolution at pH 4. Compared to their fresh counterparts in Figure 2b and 2d, respectively they demonstrate a general rounding at the edges. This is very apparent in Figure 2h, where all the sharp edges and pore rims have been rounded.

5. DISCUSSION

Roughness factors of the glass powders considered in the present study vary significantly despite the fact that they were macroscopically unaltered, and ground and cleaned before their use in dissolution experiments. Several previous studies have suggested that roughness factors tend to increase with sample age due to weathering processes (e.g., Anbeek, 1992a, 1992b, 1993; White et al., 1996; White and Brantley, 2003). A plot of

tapraid2/gca-gca/gca-gca/gca02204/gca3986d04z | xppws | S=1 | 9/16/04 | 15:00 | Art: W#2243 | DTD5.0

Table 5. Experimental results of the dissolution rate experiments at basic pH. The glasses are ordered from high to low silica content. Italic pH values were calculated from 25°C using PHREEQC

Sample	Temp. °C	Mass g	pH	Flow rate g/min	Si μmol/l	Al μmol/l	Al/Si[#]	A^* kJ/mol	log (a_H^{3+}/a_{Al}^{3+})	log $r_{+,BET}$ mol/m^2/s	log $r_{+,geo}$ mol/m^2/s
BT-2	25	1.52	10.60	0.69	20.74	3.98	0.9	21.1	−6.6	−10.30	−8.32
Ö62-1	25	1.18	10.46	1.17	4.31	0.81	0.9	25.4	−6.0	−9.78	−8.66
H1-2	25	1.18	10.62	0.95	10.06	2.70	1.2	23.9	−6.4	−9.62	−8.37
H3W-5	25	1.02	10.65	1.10	9.60	2.15	1.0	24.4	−6.3	−9.79	−8.26
A75-4	25	1.00	10.68	0.80	9.28	1.76	0.9	24.2	−6.2	−10.06	−8.41
H3B-3	25	0.81	10.64	1.13	11.63	2.70	0.4	24.4	−6.4	−9.65	−8.05
HZ0(1)-2	25	0.40	10.77	1.02	6.81	0.98	0.5	28.0	−5.8	−9.33	−8.01
HZ0(2)-3	25	0.50	10.74	1.08	7.13	2.00	1.0	27.1	−6.2	−9.38	−8.06
SLN(1)-4	25	0.41	10.76	0.80	11.59	3.36	1.1	25.2	−6.4	−9.84	−7.90
SLN(2)-4	25	0.50	10.75	1.00	8.12	2.22	1.0	26.3	−6.2	−9.99	−8.04
H20-5	25	0.27	10.69	1.03	7.23	3.74	1.7	26.7	−6.5	−8.36	−7.73
HZ1-3	25	0.25	10.63	0.85	4.76	1.71	1.1	28.5	−6.2	−9.91	−8.02
GR(1)-4	25	0.30	10.61	1.16	7.84	2.70	1.1	27.8	−6.4	−8.35	−7.71
GR(2)-5	25	0.61	10.67	1.14	13.28	4.50	1.1	26.5	−6.6	−8.43	−7.79
GR(3)-4	25	0.90	10.63	1.17	12.13	3.85	1.0	25.2	−6.6	−8.63	−7.99
HEI(1)-4	25	3.21	10.67	0.95	28.96	10.20	0.9	25.3	−7.0	−8.69	−8.28
HEI(2)-3	25	0.42	10.77	0.90	4.42	1.17	0.7	23.9	−5.9	−8.65	−8.24
A61-5	25	0.26	10.69	1.09	2.91	1.07	1.2	31.4	−6.0	−8.86	−8.11
KRA(2)-4	25	0.51	10.78	0.95	4.82	0.94	0.6	29.7	−5.8	−8.97	−8.23
KAT(2)-4	25	0.33	10.50	0.97	11.59	3.35	0.9	29.8	−6.6	−9.21	−7.64
SS(2)-8	25	1.51	10.65	1.06	30.19	11.10	0.9	24.7	−7.0	−8.74	−7.86
SS(3)-4	25	0.31	10.49	0.93	7.28	3.04	1.0	24.4	−6.6	−8.72	−7.84
ELD(3)-5	25	0.70	10.77	1.05	15.58	7.13	1.4	28.2	−6.7	−10.13	−7.81
HEI(1)-7	35	3.21	10.19	1.38	38.66	11.46	0.8	21.9	−6.5	−8.41	−7.99
KRA(2)-8	39	0.51	10.29	1.57	5.94	1.35	0.7	28.7	−5.1	−8.67	−7.92
A75-8	40	1.00	10.20	0.95	18.14	3.96	1.0	21.8	−5.6	−9.69	−8.04
H3W-8	40	1.02	10.21	1.29	21.34	5.09	1.0	21.8	−5.7	−9.38	−7.85
H3B-6	40	0.81	10.25	1.31	27.37	7.01	0.4	21.9	−5.8	−9.21	−7.62
HEI(1)-9	44	3.21	9.97	1.90	51.17	16.26	0.8	21.1	−6.0	−8.15	−7.73
KRA(2)-11	54	0.51	9.85	2.02	8.19	2.17	0.8	27.4	−4.4	−8.42	−7.67
A75-11	55	1.00	9.87	1.29	33.43	7.27	1.0	20.1	−4.8	−9.29	−7.64
H3W-11	55	1.02	9.86	1.44	51.25	12.97	1.1	19.1	−5.1	−8.95	−7.42
H3B-10	55	0.81	9.78	1.68	58.05	17.10	0.5	18.8	−5.3	−8.78	−7.18

[#] Molar $(Al/Si)_{aq}/(Al/Si)_{glass}$ ratio.

the roughness factors of the samples dissolved in the present study as a function of sample age is depicted in Figure 3. Although this figure suggests that roughness factors increase with age, a number of observations indicate that this relationship results from factors other than sample age. Basaltic eruptions have been much more common in Iceland during the recent past than rhyolitic eruptions. Rhyolitic eruptions are often associated with a violent (plinian) gas-rich eruption and the rhyolitic samples of this study come from porous pumice. The SEM images (Figs. 2c, d) reveal that all the SiO_2-rich samples other than the ignimbrite have smooth and uncoated surfaces. The high surface roughness of these samples is, therefore, likely due to primary porosity. No temporal trend is evident among the roughness factors of the rhyolitic glasses. The same applies to the basic glasses younger than 100 yr that exhibit same roughness factors within uncertainty irrespective of their age. In contrast, the oldest three basaltic glass powders do have higher roughness factors than their younger counterparts. Note however, that two of them (ELD and KAT) stem from violent hydromagmatic (i.e., by interaction of water with the magma) gas-rich eruptions, which tend to have high porosities so their high roughness factors have also contributions from porosity. Only two of these older samples (ELD and HZ1) exhibit considerable Fe coatings under the SEM.

At conditions where dissolution rates are controlled by the detachment of atoms from surfaces, these rates are believed to be proportional to the aqueous solution-surface interfacial area. BET surface areas have commonly been used to normalize dissolution rates, but there are numerous observations that suggest that for naturally weathered and porous complex compounds rates are better normalized to the geometric surface area. Some of these observations are summarized below:

The geometric surface area is a function of only the density and size of the solid (Eqn. 2). Consequently, if these two parameters are kept constant, the geometric surface area is constant. In contrast BET surface areas of many minerals have been shown to change as a function of time and sample preparation *prior* to dissolution experiments (Brantley and Chen, 1995). The comparability of BET surface normalized dissolution rates generated by different researchers or laboratories on the same material may therefore be problematical. Furthermore, analytical errors in determining the BET surface area, along with discrepancies arising by using either N_2, Kr or Ar as adsorbate gas (Brantley and Mellott, 2000), render a comparison of BET normalized dissolution rates from the literature even more ambiguous.

For natural samples, BET surface areas are affected by surface coatings, which in the case of high surface area alteration products like iron hydroxides, phyllosilicates, or organic matter, increase significantly the measured BET surface areas.

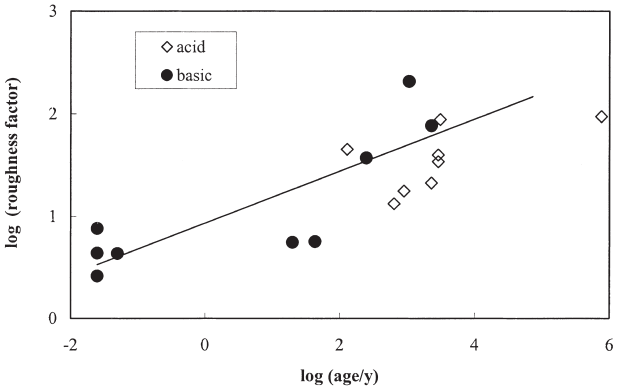

Fig. 3. Logarithms of glass powder roughness factors (A_{BET}/A_{geo}) as a function of sample age. Filled symbols represent roughness factors of basic glasses ($SiO_2 < 55$ wt.%) and open symbols represent roughness factors of acid glasses ($SiO_2 > 62$ wt.%). The line designates a linear regression of the basic glasses with a correlation coefficient (r^2) of 0.67 (see text).

The coatings may be passive or sequester the underlying reactive surface so that the resulting BET normalized dissolution rates may be substantially lower than those of the dissolving mineral. Hodson (2003) carried out dissolution experiments on anorthite powder at pH 2.6 in HCl and $FeCl_3$ solution. In the latter experiment Fe oxy-hydroxides precipitated on the anorthite surface and the specific surface area increased from 0.16 to 3.89 m^2/g. However, this coating did not affect the overall dissolution rate that was in agreement with that measured in the corresponding Fe-free system. It seems likely, however, that more pervasive coatings could potentially decrease overall dissolution rates.

BET measurements include external as well as internal surfaces, the latter being made of microstructures such as microcracks, -fractures, -vesicles, and -voids. Fluxes to and from these internal surfaces may be controlled by diffusion, thus they may not contribute significantly to the dissolution of a solid whose kinetics is surface controlled. Anbeek (1992a, 1992b, 1993) observed that the BET surface area of quartz and feldspars increases dramatically during natural weathering and that this additional BET surface area is due to internal *non-reactive* micropores.

Additionally, after taking account of the influence of non-reactive coatings and non-reactive microstructures on the BET specific surface area, the remaining BET area may still overestimate reactive surface area because not all external surfaces are reactive. For example, Gautier et al. (2001) observed that the increase in BET surface area arising during the laboratory dissolution of quartz consists of non-reactive etch pit walls and Anbeek et al. (1994) reached the same conclusion for a naturally weathered mineral assemblage of quartz and feldspar. Finally, a compilation of kinetic models reviewed by White and Peterson (1990) indicate that reactive surface areas are commonly one to three orders of magnitude *lower* than specific BET or geometric surface areas, respectively.

The observations summarized above indicate that the higher the measured BET specific surface area of naturally weathered glasses the more likely it is an overestimate of the reactive surface that is actually dissolving. This partially accounts for the discrepancy encountered when comparing BET normalized dissolution rates obtained in different laboratories. For example, the low temperature alteration rate of rhyolitic obsidian (Fiore et al., 1999) was found to differ by two orders of magnitude from that found by Karkhansis et al. (1980) under similar pH-T conditions. This discrepancy was ascribed to the fact that they normalized their rate to the BET rather than the geometric surface area of the glass. When Fiore et al. (1999) recalculated both data sets on a weight loss per gram basis, the discrepancy shrunk to a factor of only 4. Application of geometric surface areas, however, contrasts with the recommendations of Jeschke and Dreybrodt (2002) who related dissolution rates of minerals to their surface morphology. They concluded that if dissolution occurs over the entire surface, dissolution rates are best normalized to the BET specific surface area. But they also presented calculations suggesting that ink-bottle-pores, although enhancing the BET surface area, do not contribute to the dissolution rates. In such cases, dissolution rates are better normalized to geometric surface area. These findings were applied to the dissolution of calcite, gypsum, and quartz.

BET and geometric surface area normalized dissolution rates of the natural glasses considered in this study are shown as a function of their SiO_2 content in Figures 4 and 5. The filled symbols in the figures represent results obtained during this study; open symbols represent dissolution rates of natural glasses taken from the literature. The few literature data shown in these figures were chosen because these are the only data available for natural and synthetic glasses for which both BET and geometric surface area normalized rates can be retrieved at 25°C and the pH considered in these figures. The BET normalized dissolution rates of the natural glasses ($r_{+,BET}$) range over more than two orders of magnitude at both acid and basic pH. Although a trend of lower $r_{+,BET}$ with increasing SiO_2 is apparent there is much scatter, especially for SiO_2 poor glasses. A linear least square fit of log $r_{+,BET}$ with the silica content is provided on Figures 4a and 5a. These fits confirm a decrease in rates with decreasing Si content. The fits however, are relatively poor. At pH 4 and 10.6 correlation coefficients[1] (r^2) are 0.60 and 0.36, respectively. The pH 4 regression line reproduces only 19 of the 25 measured rates within uncertainty while the pH 10.6 line reproduces only 11 of the 23 measured rates within uncertainty. In contrast, the corresponding least square fits of the geometric surface area normalized dissolution rates ($r_{+,geo}$) with the silica content are significantly better. At pH 4 this linear regression is given by:

$$\log r_{+,geo}(mol/m^2/s) = -0.03 \cdot [SiO_2(wt\%)] - 7.58 \quad (7)$$

r^2 is 0.75, and *all* of the 25 measured rates match this regression line within uncertainty. At pH 10.6 the regression is given by:

$$\log r_{+,geo}(mol/m^2/s) = -0.02 \cdot [SiO_2(wt\%)] - 7.02 \quad (8)$$

[1] Regressions were computed in the present study using Microsoft EXCEL. This program calculates the square of the Pearson product moment correlation coefficient, which can be inverted to yield the proportion of the variance in y attributable to the variance in x. This goodness of fit parameter is referred to in this study as the correlation coefficient.

tapraid2/gca-gca/gca-gca/gca02204/gca3986d04z | xppws | S=1 | 9/16/04 | 15:00 | Art: W#2243 | DTD5.0

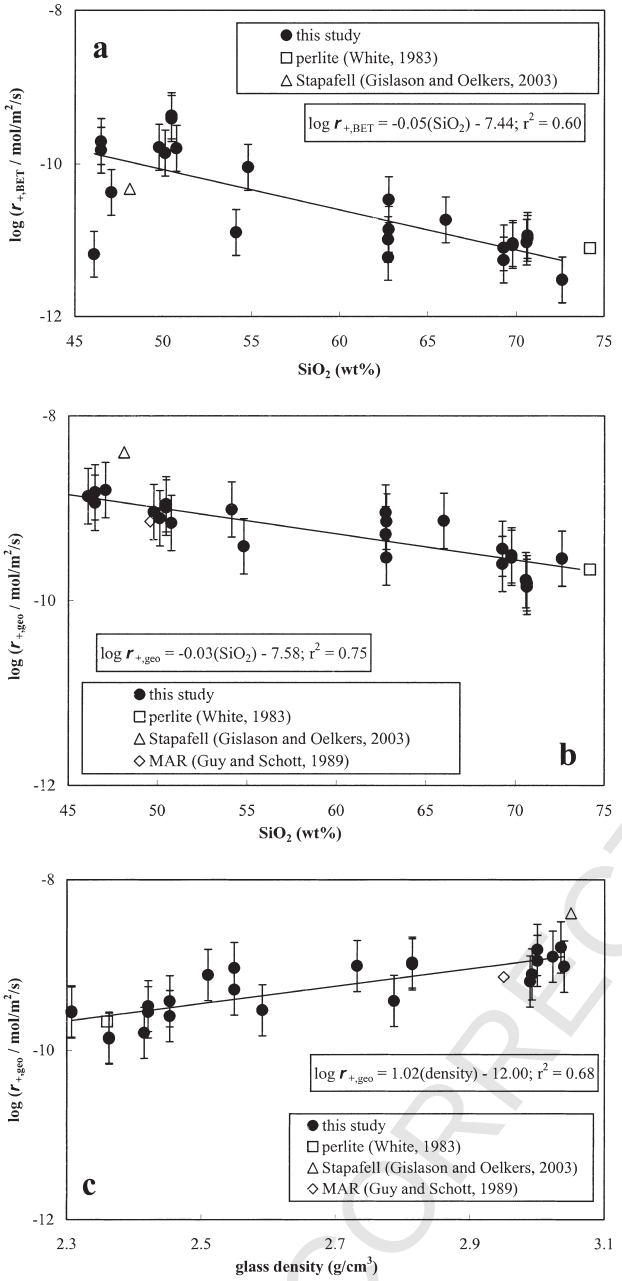

Fig. 4. Logarithm of dissolution rates versus the silica content of the glasses and their densities at pH 4 and 25°C: (a) BET normalized dissolution rates, (b) geometric surface area normalized dissolution rates, (c) geometric surface area normalized dissolution rates versus the glass densities. The symbols correspond to measured rates and from the references listed in the legend. The lines through the data represent a linear least square fit; the equations and correlation coefficients (r^2) of these fits are provided in the figure.

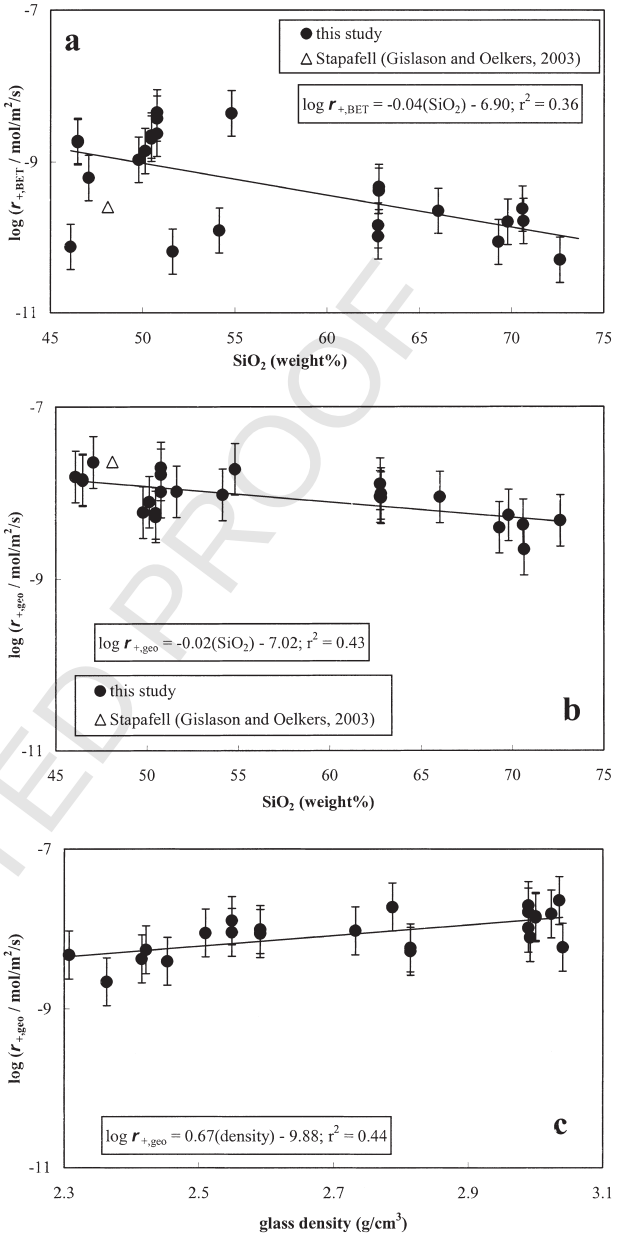

Fig. 5. Logarithm of dissolution rates versus the silica content of the glasses and their densities at pH 10.6 ± 0.2 and 25°C: (a) BET normalized dissolution rates, (b) geometric surface area normalized dissolution rates, (c) geometric surface area normalized dissolution rates versus the glass densities. The symbols correspond to measured rates and from the references listed in the legend. The lines through the data represent a linear least square fit; the equations and correlation coefficients (r^2) of these fits are provided in the figure.

r^2 is 0.43 and 21 of the 23 measured rates match this regression line within uncertainty. Note that as glass density decreases with increasing Si content, glass dissolution rates will also be functions of glass density. This relation is explored in Figures 4c and 5c, where $r_{+,geo}$ is plotted against the density of each glass sample. A strong correlation is observed, and the slope of this linear correlation is close to 1 for pH 4, suggesting that the quotient $r_{+,geo}/\rho$ is close to constant at acid to subneutral pH.

The close correspondence between the line and symbols in Figures 4b and 5b demonstrates that far-from-equilibrium dissolution rates, normalized to the geometric surface area, can be predicted at pH 4 and 10.6 and 25°C for natural glasses of variable composition. Note that these correlations also describe accurately dissolution rates of other natural glasses taken from the literature, which were performed using different experimen-

tapraid2/gca-gca/gca-gca/gca02204/gca3986d04z | xppws | S=1 | 9/16/04 | 15:00 | Art: W#2243 | DTD5.0

tal methods. This observation strongly supports the application of Eqn. 7 and (8) to the description of natural glass dissolution rates. As noted above, basaltic glass dissolution rates have been demonstrated to vary with aqueous solution composition in accord with $(a_{H}^{3+}/a_{Al}^{3+})^{1/3}$ (Oelkers and Gislason, 2001; Gislason and Oelkers, 2003). The degree to which this dependence holds for other glass compositions is unclear, but to assure that it does not affect the comparisons shown in Figures 4 and 5 the (a_{H}^{3+}/a_{Al}^{3+}) activity ratios were held close to constant in the experimental results shown in these figures (see above).

Several authors have reported a compositional dependence of dissolution rates for natural and synthetic glasses on their respective chemical composition. For example, Karkhanis et al. (1980) found that leach rates of rhyolite glass disks were 3–10 times greater than those for borosilicate glass disks. Allnatt et al. (1983), in a similar study, reported an order of magnitude difference between borosilicate and rhyolite glass leach rates. A comparison of the leached layer thickness of basaltic, rhyolitic, and borosilicate glass performed by Petit et al. (1990) suggests that the corrosion resistance is highest for the rhyolite glass. Shoji et al. (1993) found that laboratory dissolution rates of "coloured glass" of basaltic andesite composition are 1.5 times higher than that of "non-coloured glass" of rhyolitic composition. All these investigations corroborate that glass dissolution rates increase with decreasing Si content, yet a numerical relationship had not been previously generated. This may be due to ambiguities stemming from the use of BET normalized dissolution rates in these studies. The scatter among the data points in Figures 4a and 5a illustrates the difficulty in defining an unambiguous trend among these BET normalized rates. Such is not the case for geometric surface area normalized rates as illustrated in Figures 4b and 5b. A linear relationship between the logarithmic dissolution rates and silica content has been previously suggested. Jantzen and Plodinec (1984) performed batch dissolution experiments at 90°C and neutral pH on an array of polished glass disks (MCC-1 test procedure) ranging in composition from pure SiO_2 to borosilicate glass. They found a linear relationship between the logarithm of the normalized mass loss of Si and the free energy of hydration, ΔG_{hyd}. The free energy of hydration was assumed to be the sum of the hydration stabilities of the major oxides weighted by their mole fraction in the glass (Paul, 1982). Since SiO_2 is by far the most important glass oxide in natural glasses, Jantzen and Plodinec (1984) effectively found that the logarithm of their glass dissolution rates decreased linearly with the Si content. Perret et al. (2003) reached a similar conclusion in their investigation on the thermodynamic stability of waste glasses. They demonstrated that Si and Ca contents control the glass' thermodynamic stability; the latter element indirectly by governing the pH during corrosion experiments whereas silicon directly influences the glass durability. However, their relationship between ΔG_{hyd} and logarithmic normalized apparent dissolution rates is less linear and changes with corrosion time.

The results, described by Eqn. 7 and (8), make it possible to estimate the lifetime of natural glasses at pH 4, 25°C and far-from-equilibrium conditions. The time t required to completely dissolve a spherical grain is given by (Lasaga, 1998):

$$t_{\text{lifetime}} = \left(\frac{rad}{V_m r_{+,\text{geo}}} \right) \quad (9)$$

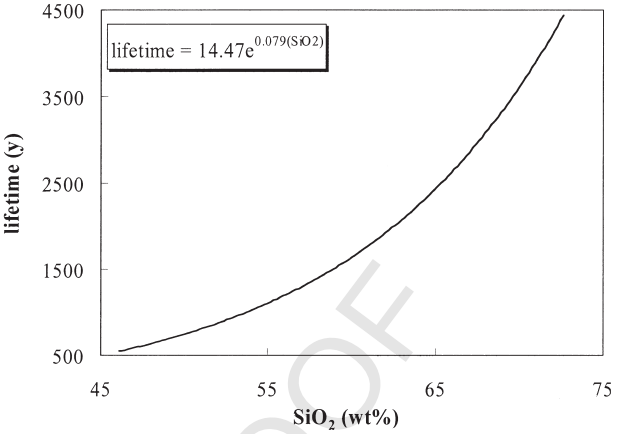

Fig. 6. Calculated lifetimes of 1mm radius natural glass spheres as a function of their silica content at 25°C and pH 4.

where rad stands for the grain radius and V_m refers to the molar volume where a mole of glass is assumed to contain one Si atom. The lifetime of a 1 mm radius spherical glass grain was computed by combining Eqn. 7 and (9); the result of this calculation is illustrated in Figure 6. A 1 mm radius basaltic glass grain has a lifetime of 500 yr. The lifetime increases exponentially with increasing Si content; a 1 mm radius rhyolite glass grain has a lifetime of 4500 yr. These results can be compared with those of glasses in natural environments. Ruxton (1988) studied the weathering of andesite ash in Papua New Guinea. According to his results, a 1 mm radius andesite glass sphere has a lifetime of 60–100 yr under subneutral pH conditions, depending on the soil thickness and depth. This value is approximately 20 times smaller than that estimated from rates measured in this study (Fig. 6). This difference may stem from differences in solution composition including pH and the presence of aqueous organic acids. For example, Oelkers and Gislason (2001) noted that addition of 1 mM oxalic acid at pH 4.5 and 25°C increases the dissolution rate of basaltic glass by a factor of 50. Rowe and Brantley (1993) estimated a lifetime of a 1 mm radius andesitic glass grain to be 90000 yr in a Costa Rican aquifer, at acid pH. This value is 50 times greater than that estimated in the present study, however, Rowe and Brantley (1993) report that their value has an uncertainty of ±1.8 log units.

It should be emphasized that the predicted lifetimes shown in Figure 6 were computed for natural glass grains in solutions that are far-from-equilibrium from the dissolving glass. Although such conditions may be rare in the crust and in soils, they are common on the Earth's surface. PHREEQC calculations performed on a variety of natural surface waters including average world river (Meybeck, 1979; Martin and Whitfield, 1983), an average Icelandic river (Gislason et al., 1996), an Icelandic lake (Gislason et al., 2003), and average ocean water (Stumm and Morgan, 1996) indicate that all these waters are far-from-equilibrium with respect to all the hydrated volcanic glasses compiled in Table 1 (cf. chapter 2).

Natural glass dissolution rates generated in the present study also allow estimation of the nutrient fluxes due to glass dissolution in glass bearing soils at pH = 4 and 25°C and far-from-equilibrium conditions. These fluxes can be computed using:

tapraid2/gca-gca/gca-gca/gca02204/gca3986d04z | xppws | S=1 | 9/16/04 | 15:00 | Art: W#2243 | DTD5.0

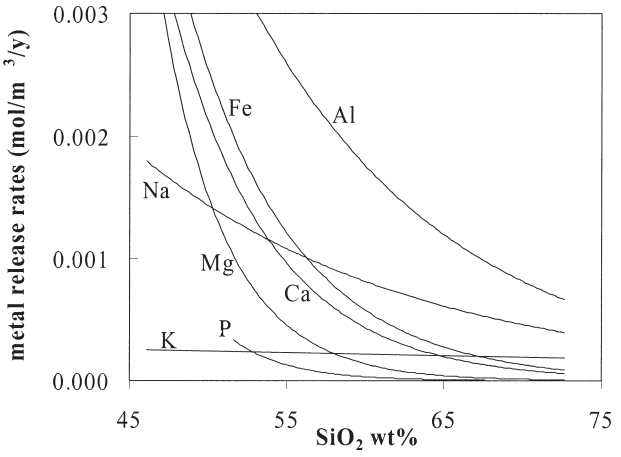

Fig. 7. Metal release rates from natural glasses as a function of their silica content at 25°C and pH 4. These calculations were performed assuming a soil thickness of 1m, a glass fraction of 0.7, and a porosity of 0.2.

$$F_i = \frac{r_{+,geo}\delta_i\rho\chi}{L} \quad (10)$$

where F_i designates the flux of the ith element, δ_i stands for a stoichiometric coefficient equal to the number of moles of the ith element in one mole of the glass, ρ denotes the porosity of the soil, χ symbolizes the glass fraction in the soil, and L represents the thickness of the soil horizon. Eqn. 9 was used to estimate F_i for a soil with a porosity of 0.2, a glass fraction of 0.7, and a soil thickness of 1 m. Fluxes were computed for each individual glass listed in Tables 1 and 2 using rates listed in Table 4. The results of this estimation are represented by the curves in Figure 7. These curves correspond to a fit of the individually computed fluxes for each of the glasses. Note the fluxes illustrated in this figure are based on the assumption of stoichiometric glass dissolution; secondary phases are assumed not to precipitate. To increase the figure resolution, Si release rates, which exceed that of Al, are not shown. Metal release rates decrease exponentially with increasing Si content for most metals. Phosphorous follows exponential release behaviour to a SiO_2 content $\geq$51 wt.% but the more basic glasses have inconsistent F_P values ranging from 4 to $16 \cdot 10^{-5}$ mol/m^3/yr. The release flux of potassium is independent of the Si content of the glass because the weight percentage of K_2O increases steadily from basaltic to rhyolitic glass cancelling out the inverse dissolution rate effect. These results are consistent with the increased fertility of volcanic soils with decreasing Si content (Dahlgren et al., 1993).

6. EXPERIMENTAL AND COMPUTATIONAL UNCERTAINTIES

Uncertainties associated with the rate constants generated in the present study arise from a variety of sources, including the measurement of aqueous solution concentrations, glass composition, fluid flow rates, and the determination of the specific glass surface areas. Errors in the measured values of the total aqueous silica and aluminium concentration are estimated to be on the order of $\leq$10%. The experimental error in measured pH is $\pm$0.05 pH units and uncertainties in fluid flow rate measurements are less than 5%. In contrast, uncertainties associated with the BET determination of the specific surface area of the glass powders are considered $\pm$10%. If the error propagation is estimated from the sum of these contributions, an overall uncertainty of the $r_{+,BET}$ listed in Table 4 will be ~25% ($\cong$0.1 log units). This estimate is in very good agreement with the scatter among dissolution rates obtained from a single long-term steady state experiment (Fig. 1). However, repeated experiments yield log $r_{+,BET}$ values that vary by as much as 0.25 log units. Thus, an overall error of $\pm$0.3 log units is apparently associated with the log $r_{+,BET}$ values.

Uncertainties related to $r_{+,geo}$ originate from essentially the same sources. The only difference stems from uncertainties associated with computing A_{geo}. A_{geo} is determined mathematically and the uncertainty associated with it depends on a) how close the effective particle diameter is to the actual average particle diameter and b) how close the particle density is to the bulk density of the vesicular glasses. It seems likely that these combined uncertainties do not exceed $\pm$10% and thus the uncertainties on $r_{+,geo}$ are approximately equal to those of $r_{+,BET}$.

7. CONCLUSIONS

Both BET and geometric surface area normalized dissolution rates of natural glasses are found to decrease with their silica content. Linear regressions between the logarithm of measured rates and the silica content of the glasses are far stronger for geometric rather than BET normalized rates. This observation likely stems from the fact that BET surface areas include the contribution of non-Si bearing surface coatings and non-reactive surfaces. The cogent correlation between the logarithm of geometric surface area normalized natural glass dissolution rates with their Si content provides a powerful tool for the prediction of the behaviour of natural glasses in both natural and industrial processes. Two examples of such predictions are provided in the present study; 1) the lifetimes of 1 mm radius glass spheres at pH 4, 25°C, and in far-from-equilibrium solutions increases from 500 to 4500 yr with increasing Si content from basaltic to rhyolitic glass and 2) nutrient release fluxes are predicted to decrease exponentially with increasing Si content. Experiments in this study illustrate the systematics of natural glass dissolution rates with their composition at pH 4 and 10.6, and 25°C. The degree to which this systematics also holds for other solution compositions and the degree to which the dissolution mechanism of natural glasses depends on their composition are further explored in Wolff-Boenisch et al. (2004).

Acknowledgments—We would like to thank Marijo Murillo, Malla Kristiansen, and Stacey Callahan for their personal support during the course of this study. Helpful discussions and constructive comments were generously provided by Eydis Eiriksdottir, Athanasios Godelitsas, Ingvi Gunnarsson, David Heasman, Björn Jamtveit, Stephan Kohler, Gudrun Larsen, Manuel Prieto, Andrew Putnis, Vala Ragnarsdottir, Olga Riba, and Olgeir Sigmarsson. Bergur Sigfusson contributed essentially to the design and manufacturing of own flow-through reactors. The authors express their thanks also to Nora Groschopf of the Mineralogy-Geochemistry department of the Johannes Gutenberg University, Mainz, who conducted the XRF analyses of the natural glasses. Thanks also to Don Voight from Pennsylvania State University for carrying out the BET measurements on the glasses. This manuscript greatly benefited from critical reviews by Susan Brantley, Jean-Louis

tapraid2/gca-gca/gca-gca/gca02204/gca3986d04z | xppws | S=1 | 9/16/04 | 15:00 | Art: W#2243 | DTD5.0

Crovisier, the associate editor Roy Wogelius and an anonymous reviewer.

This study has been financed by the European Union through a Research Training Network titled "Quantifying the dissolution and precipitation of solid solutions in natural and industrial processes" within the 5th framework programme (contract number: HPRN-CT-2000-00058) and the Science Institute, University of Iceland.

Associate editor: R. Wogelius

REFERENCES

Aagard P. and Helgeson H. C. (1982) Thermodynamic and kinetic constraints on reaction rates among minerals and aqueous solutions, I. Theoretical considerations *Am. J. Sci.* **282,** 237–285.

Abraitis P. K., McGrail B. P., Trivedi D. P., Livens F. R. and Vaughan D. J. (2000) Single-pass flow-through experiments on a simulated waste glass in alkaline media at 40°C. II. Experiments conducted with buffer solutions containing controlled quantities of Si and Al *J. Nucl. Mater.* **280,** 206–215.

Advocat T., Crovisier J. L., Fritz B. and Vernaz E. (1990) Thermokinetic model borosilicate glass dissolution: contextual affinity. *Mater. Res. Soc. Symp. Proc.* **176,** 241–248.

Advocat T., Crovisier J. L., Vernaz E., Ehret G. and Charpentier H. (1991) Hydrolysis of R7T7 nuclear waste glass in dilute media: mechanisms and rate as a function of pH. *Mater. Res. Soc. Symp. Proc.* **212,** 57–64.

Advocat T., Chouchan J. L., Crovisier J. L., Guy C., Daux V., Jegou C., Gin S. and Vernaz E. (1998) Borosilicate nuclear waste glass alteration kinetics: chemical inhibition and affinity control. *Mater. Res. Soc. Symp. Proc.* **506,** 63–70.

Alkattan M., Oelkers E. H., Dandurand, J. L. and Schott, J. (1997) Experimental studies of halite dissolution kinetics. 1. The effect of saturation state and the presence of trace metals. *Chem. Geol.* **137,** 201–219.

Allen C. C. (1982) Stability and alteration of naturally occurring low-silica glasses: implications for the long-term stability of waste form glasses. *Mater. Res. Soc. Symp. Proc.* **11,** 37–44.

Allnatt A. R., Bancroft G. M., Fyfe W. S., Jacobs P. W. M., Karkhanis S. N., Melling P. J., Nishijima A., Vempati C. S. and Tait J. (1983) Leaching behaviour and electrical conductivity of natural rhyolite and modified synthetic rhyolites. *Chem. Geol.* **38,** 329–357.

Alt J. C. and Teagle D. A. H. (1999) The uptake of carbon during alteration of ocean crust. *Geochim. Cosmochim. Acta* **63,** 1527–1535.

Alt J. C., Honnores J., Laverne C., and Emmermann R. (1986) Hydrothermal alteration of a 1 km section through the upper oceanic crust. Deep Sea Drilling Project Hole 504B: Mineralogy, chemistry, and evolution of seawater-basalt interactions *J. Geophys. Res.* **91,** 10309–10335.

Anbeek C. (1992a) Surface roughness for minerals and implications for dissolution studies. *Geochim. Cosmochim. Acta* **56,** 1461–1469.

Anbeek C. (1992b) The dependence of dissolution rates on grain size for some fresh and weathered feldspars. *Geochim. Cosmochim. Acta* **56,** 3957–3970.

Anbeek C. (1993) The effect of natural weathering on dissolution rates. *Geochim. Cosmochim. Acta* **57,** 4963–4975.

Anbeek C., van Breemen N., Meijer E. L., and van der Plas L. (1994) The dissolution of naturally weathered feldspar and quartz. *Geochim. Cosmochim. Acta* **58,** 4601–4614.

Berger G., Schott J. and Loubet M. (1987) Fundamental processes controlling the first stage of alteration of a basaltic glass by seawater: An experimental study between 200 and 320°C. *Earth Planet. Sci. Lett.* **84,** 431–445.

Berger G., Schott J. and Guy C. (1988) Behaviour of Li, Rb, and Cs during basalt glass and olivine dissolution and chlorites, smectites and zeolites precipitation from seawater: Experimental investigation and modelization between 50°C and 300°C. *Chem. Geol.* **71,** 297–312.

Berger G., Claparols C., Guy C. and Daux V. (1994) Dissolution rate of a basalt glass in silica-rich solutions: Implications for long-term alteration. *Geochim. Cosmochim. Acta* **58,** 4875–4886.

Bottinga Y. A. and Weil D. F. (1972) The viscosity of magmatic silicate liquids: a model for calculation. *Am. J. Sci.* **272,** 438–473.

Bourcier W. L., Peiffer D. W., Knauss K. G., McKeegan K. D. and Smith D. K. (1990) A kinetic model for borosilicate glass dissolution based on the dissolution affinity of a surface alteration layer. *Mat. Res. Soc. Symp. Proc.* **176,** 209–216.

Brady P. V. (1991) The effect of silicate weathering on global temperature and atmospheric CO_2. *J. Geophys. Res.* **86,** 18101–18106.

Brady P. V. and Gislason S. R. (1997) Seafloor weathering controls on atmospheric CO_2 and global climate. *Geochim. Cosmochim. Acta* **61,** 965–973.

Brantley S. L. and Chen Y. (1995) Chemical weathering rates of pyroxenes and amphibols. In *Chemical weathering rates of silicate minerals* (eds. A. F. White and S. L. Brantley) *Rev. Mineral.* **31,** 119–172.

Brantley S. L., White A. F. and Hodson M. (1999) Surface area of primary silicate minerals. In *Growth, dissolution and pattern formation in geosystems* (eds. Jamtveit B. and P. Meakin), pp. 291–326. Kluwer Academic Publishers.

Brantley S. L. and Mellott N. P. (2000) Surface area and porosity of primary silicate minerals. *Am. Mineral.* **85,** 1767–1783.

Byers C. D., Jercinovic M. J., Ewing R. C. and Keil K. (1985) Basalt glass: an analogue for the evaluation of the long-term stability of nuclear waste form borosilicate glasses. *Mater. Res. Soc. Symp. Proc.* **44,** 583–590.

Caldeira K. (1995) Long-term control of atmospheric carbon dioxide: Low-temperature seafloor alteration or terrestrial silicate rock weathering? *Am. J. Sci.* **295,** 1077–1114.

Carey S. N. (1997) Influence of convective sedimentation on the formation of widespread tephra fall layers in the deep sea. *Geology* **25,** 839–842.

Chadwick O. A. and Chorover J. (2001) The chemistry of pedogenic thresholds. *Geoderma* **100,** 321–353.

Crovisier J. L., Thomassin J. H., Juteau T., Eberhart J. P., Touray J. C. and Baillif P. (1983) Experimental seawater–basaltic glass interaction at 50°C: study of early developed phases by electron microscopy and X-ray photoelectron spectrometry. *Geochim. Cosmochim. Acta* **47,** 377–387.

Crovisier J. L, Fritz B., Grambow B. and Eberhart J. P. (1985) Dissolution of basaltic glass: experiments and thermodynamic modelling. *Mater. Res. Soc. Symp. Proc.* **50,** 273–280.

Crovisier J. L., Honnorez J. and Eberhart J. P. (1987) Dissolution of basaltic glass in seawater: Mechanism and rate. *Geochim. Cosmochim. Acta* **51,** 2977–2990.

Crovisier J. L., Atassi H., Daux V., Honnorez J., Petit J. C., and Eberhart J. P. (1989a) A new insight into the nature of the leached layers formed on basaltic glasses in relation to the choice of constraints for long-term modeling. *Mater. Res. Soc. Symp. Proc.* **127,** 41–48.

Crovisier J. L., Advocat T., Petit J. C. and Fritz B. (1989b) Alteration of basaltic glass in Iceland as natural analogue for nuclear waste glasses: geochemical modelling with DISSOL. *Mater. Res. Soc. Symp. Proc.* **127,** 57–64.

Dahlgren R., Shoji S. and Nanzyo M. (1993) Mineralogical characteristics of volcanic ash soils. In *Volcanic ash soils. Genesis, Properties, and Utilization* (eds. Shoji, S. Nanzyo M. and Dahlgren R.) pp. 101–143. Elsevier, Amsterdam.

Dahlgren R. A., Ugolini F. C. and Casey W. H. (1999) Field weathering rates of Mt. St. Helens tephra. *Geochim. Cosmochim. Acta* **63,** 587–598.

Daux V., Crovisier J. L., Hemond C. and Petit J. C. (1994) Geochemical evolution of basaltic rocks subjected to weathering: fate of the major elements, rare earth elements, and thorium. *Geochim. Cosmochim. Acta* **58,** 4941–4954.

Daux V., Guy C., Advocat T., Crovisier J. L. and Stille P. (1997) Kinetic aspects of basaltic glass dissolution at 90°C: Role of aqueous silicon and aluminium. *Chem. Geol.* **142,** 109–126.

Dickin A. P. (1981) Hydrothermal leaching of rhyolite glass in the environment has implications for nuclear waste disposal. *Nature* **294,** 342–347.

Dove P. M. and Crerar D. A. (1990) Kinetics of quartz dissolution in electrolyte solutions using a hydrothermal mixed flow reactor. *Geochim. Cosmochim. Acta* **54,** 955–969.

AQ: 1

tapraid2/gca-gca/gca-gca/gca02204/gca3986d04z | xppws | S=1 | 9/16/04 | 15:01 | Art: W#2243 | DTD5.0

Dran J.-C., Petit J.-C. and Brousse C. (1986) Mechanism of aqueous dissolution of silicate glasses yielded by fission tracks. *Nature* **319,** 485–487.

Dran J.-C., Della Mea G., Paccagnella A., Petit J.-C. and Trotignon L. (1988) The aqueous dissolution of alkali silicate glasses: reappraisal of mechanisms by H and Na depth profiling with high energy ion beams. *Phys. Chem. Glasses* **29,** 249–255.

Eggleton R. A., Foudoulis C. and Farkevisser D. (1987) Weathering of basalt: changes in rock chemistry and mineralogy. *Clays Clay Min.* **35,** 161–169.

Ewing R. C, Haaker R. F (1979) Naturally occurring glasses: analogues for radioactive waste forms. Battelle Report PNL-2776/UC-70.

Fiore S., Huertas F. J., Tazaki K., Huertas F. and Linares J. (1999) A low temperature experimental alteration of a rhyolitic obsidian. *Eur. J. Mineral.* **11,** 455–469.

Fishman M. J. and Friedman L. C. (eds.) (1989) Techniques of water-resources investigations of the United States Geological Survey. Methods for determination of inorganic substances in water and fluvial sediments. Book 5, Chap. A1. United States Department of the Interior.

Francois L. M. and Walker J. C. G. (1992) Modelling the phanerozoic carbon cycle and climate: constraints from the $^{87}Sr/^{86}Sr$ isotopic ratio of seawater. *Am. J. Sci.* **292,** 81–135.

Furnes H. (1975) Experimental palagonitization of basaltic glasses of varied composition. *Contrib. Mineral. Petrol.* **50,** 103–113.

Furnes H. (1978) Element mobility during palagonitization of a subglacial hyaloclastite in Iceland. *Chem. Geol.* **22,** 249–264.

Gautier J.-M., Oelkers E. H., and Schott J. (1994) Experimental study of K-feldspar dissolution rates as a function of chemical affinity at 150°C and pH 9. *Geochim. Cosmochim. Acta* **58,** 4549–4560.

Gautier J.-M., Oelkers E. H. and Schott J. (2001) Are quartz dissolution rates proportional to BET surface areas? *Geochim. Cosmochim. Acta* **65,** 1059–1070.

Ghiara M. R., Franco E., Petti C., Stanzione D. and Valentino G. M. (1993) Hydrothermal interaction between basaltic glass, deionized water and seawater. *Chem. Geol.* **104,** 125–138.

Gislason S. R. and Eugster H. P. (1987a) Meteoric water-basalt interactions: I. A laboratory study. *Geochim. Cosmochim. Acta* **51,** 2827–2840.

Gislason S. R. and Eugster H. P. (1987b) Meteoric water-basalt interactions: II. A field study in NE Iceland *Geochim. Cosmochim. Acta* **51,** 2841–2855.

Gislason S. R., Veblen D. R. and Livi K. J. T. (1993) Experimental meteoric water–basalt interactions: characterization and interpretation of alteration products. *Geochim. Cosmochim. Acta* **57,** 1459–1471.

Gislason S. R., Arnórsson S. and Ármannsson H. (1996) Chemical weathering of basalt in SW Iceland: effects of runoff, age of rocks and vegetative/glacial cover. *Am. J. Sci.* **296,** 837–907.

Gislason S. R. and Oelkers E. H. (2003) The mechanism, rates, and consequences of basaltic glass dissolution: II. An experimental study of the dissolution rates of basaltic glass as a function of pH at temperatures from 6°C to 150°C. *Geochim. Cosmochim. Acta* **67,** 3817–3832.

Gislason S. R., Eiríksdóttir E. S., Elefsen S. Ó., Hardardóttir J. and Torssander P. (2003) Chemical monitoring of the outlet from Lake Mıvatn in 1998–1999. Internal report of the Myvatn Research Station, in press.

Grambow B. (1985) A general rate equation for nuclear waste glass corrosion. *Mat. Res. Soc. Symp. Proc.* **44,** 15–27.

Grambow B., Jercinovic M. J., Ewing R. C. and Byers C. D. (1985) Weathered basalt glass: a natural analogue for the effects of reaction progress on nuclear waste glass alteration. *Mater. Res. Soc. Symp. Proc.* **50,** 263–272.

Guy C. and Schott J. (1989) Multisite surface reaction versus transport control during hydrolysis of a complex oxide. *Chem. Geol.* **78,** 181–204.

Haflidason H., Eiriksson J. and Van Kreveld S. (2000) The tephrochronology of Iceland and the North Atlantic region during the Middle and Late Quaternary: a review. *J. Quaternary Sci.* **15,** 3–22.

Helgeson H. C., Murphy W. M. and Aagaard P. (1984) Thermodynamic and kinetic constraints on reaction rates among minerals and aqueous solutions. II. Rate constants, effective surface area, and the hydrolysis of feldspar *Geochim. Cosmochim. Acta* **48,** 2405–2432.

Hildreth W. (1979) The Bishop Tuff: Evidence for the origin of compositional zonation in silicic magma chambers. In *Ashflow Tuffs* (eds. Chapin C. E. and W. E. Elston), pp. 43–75. Geol. Soc. Am. Spec. Paper 180.

Hodson M. E. (2003) The influence of Fe-rich coatings on the dissolution of anorthite at pH 2.6. *Geochim. Cosmochim. Acta*, in press.

Jantzen C. M. and Plodinec M. J. (1984) Thermodynamic model of natural, medieval and nuclear waste glass durability. *J. Non-Cryst. Solids* **67,** 207–223.

Jaycock M. J. and Parfitt G. D. (1981) Chemistry of interfaces. E. Horwood, Chichester.

Jercinovic M. J., Kaser S. A., Ewing R. E. and Lutze W. (1990a) Comparison of surface layers formed on synthetic basaltic glass, French R7T7 and HMI borosilicate nuclear waste form glasses—materials interface interactions tests, waste isolation pilot plant. *Mater. Res. Soc. Symp. Proc.* **176,** 355–362.

Jercinovic M. J., Keil K., Smith M. R. and Schmitt R. A. (1990b) Alteration of basaltic glasses from north-central Br. Columbia, Canada. *Geochim. Cosmochim. Acta* **54,** 2679–2696.

Jeschke A. A. and Dreybrodt W. (2002) Dissolution rates of minerals and their relation to surface morphology. *Geochim. Cosmochim. Acta* **66,** 3055–3062.

Karkhansis S. N., Bancroft G. M., Fyfe W. S. and Brown J. D. (1980) Leaching behaviour of rhyolite glass. *Nature* **284,** 435–437.

Kump L. R., Brantley S. L. and Authur M. A. (2000) Chemical weathering, atmospheric CO_2, and Climate. *Ann. Rev. Earth Planet. Sci.* **28,** 611–667.

Lacasse C. and van den Bogaard P. (2002) Enhanced airborne dispersal of silicic tephras during the onset of northern hemisphere glaciations, from 6 to 0 Ma records of explosive volcanism and climate change in the subpolar North Atlantic. *Geology* **30,** 623–626.

Larsen G., Newton A. J., Dugmore A. J., and Vilmundardottir E. G. (2001) Geochemistry, dispersal, volumes and chronology of Holocene silicic tephra layers from the Katla volcanic system, Iceland. *J. Quat. Sci.* **16,** 119–132.

Lasaga A. C. (1981) Transition state theory. In *Kinetics of geochemical processes* (eds. A. C. Lasaga and R. J. Kirckpatrick). *Rev. Mineral.* **8,** 135–169.

Lasaga A. C. (1998) Kinetic theory in Earth Sciences. Princeton University Press, New Jersey.

Leturcq G., Berger G., Advocat T. and Vernaz E. (1999) Initial and long-term dissolution rates of aluminosilicate glasses enriched in Ti, Zr and Nd. *Chem. Geol.* **160,** 39–62.

Lutze W., Malow G., Ewing R. C., Jercinovic M. J. and Keil K. (1985) Alteration of basalt glasses: implications for modeling the long-term stability of nuclear waste glasses. *Nature* **314,** 252–255.

Magonthier M.-C., Petit J.-C. and Dran J.-C. (1992) Rhyolitic glasses as natural analogues of nuclear waste glasses: Behaviour of an Icelandic glass upon natural aqueous corrosion. *Appl. Geochem. Supp.* **1,** 83–93.

Malow G., Lutze W. and Ewing R. C. (1984) Alteration effects and leach rates of basaltic glasses: implications for the long-term stability of the nuclear waste form borosilicate glasses. *J. Non-Cryst. Solids* **67,** 305–321.

Martin J.-M. and Whitfield M. (1983) The significance of the river input of chemical elements to the ocean. In *Trace metals in seawater* (eds. C. S. Wong, E. Boyle, K. W. Bruland, Burton J. D. and Goldberg E. D.) pp. 265–296. Plenum, New York.

Mazer J. J. and Walter J. V. (1994) Dissolution kinetics of silica as a function of pH between 40 and 85°C. *J. Non-Cryst. Solids* **170,** 32–45.

Metz V. and Ganor J. (2001) Stirring on kaolinite dissolution rate. *Geochim. Cosmochim. Acta* **65,** 3475–3490.

Meybeck M. (1979) Concentrations des eaux fluviales en éléments majeurs et apports en solutions aux océans. *Rev. Géol. Dyn. Géogr. Phys.* **21,** 215–246.

Morgan N. A. and Spera F. J. (2001) Glass transition, structural relaxation, and theories of viscosity: A molecular dynamics study of amorphous $CaAl_2Si_2O_8$. *Geochim. Cosmochim. Acta* **65,** 4019–4041.

AQ: 2

AQ: 3

tapraid2/gca-gca/gca-gca/gca02204/gca3986d04z | xppws | S=1 | 9/16/04 | 15:01 | Art: W#2243 | DTD5.0

Morgenstein M. E. and Shettel D. L. (1994) Volcanic glass as a natural analog for borosilicate waste glass. *Mater. Res. Soc. Symp. Proc.* **333,** 15–27.

Mungall J. E. and Martin R. F. (1994) Severe leaching of trachyte glass without devitrification, Terceira, Azores. *Geochim. Cosmochim. Acta* **58,** 75–83.

Murphy W. M., Oelkers E. H. and Lichtner P. C. (1989) Surface reaction versus diffusion control of mineral dissolution and growth rates in geochemical processes. *Chem. Geol.* **78,** 357–380.

Murukami T., Banba T., Jercinovic M. J. and Ewing R. E. (1989) Formation and evolution of alteration layers on borosilicate and basalt glasses: initial stage. *Mater. Res. Soc. Symp. Proc.* **127,** 65–72.

Nesbitt H. W. and Young G. M. (1984) Prediction of some weathering trends of plutonic and volcanic rocks based on thermodynamic and kinetic considerations. *Geochim. Cosmochim. Acta* **48,** 1523–1534.

Nesbitt H. W. and Wilson R. E. (1992) Recent chemical weathering of basalts. *Am. J. Sci.* **292,** 740–777.

Oelkers E. H., Schott J. and Devidal J.-L. (1994) The effect of aluminium, pH, and chemical affinity on the rates of aluminosilicate dissolution reactions. *Geochim. Cosmochim. Acta* **58,** 2011–2024.

Oelkers E. H. (2001) A general kinetic description of multi-oxide silicate mineral and glass dissolution. *Geochim. Cosmochim. Acta* **65,** 3703–3719.

Oelkers E. H. and Gislason S. R. (2001) The mechanism, rates, and consequences of basaltic glass dissolution: I. An experimental study of the dissolution rates of basaltic glass as a function of aqueous Al, Si, and oxalic acid concentration at 25°C and pH = 3 and 11 *Geochim. Cosmochim. Acta* **65,** 3671–3681.

Parkhurst D. L, Appelo C. A. J (1999) User's guide to PHREEQC (Version 2)—A computer program for speciation, batch-reaction, one-dimensional transport, and inverse geochemical calculations. *U. S. G. S. Wat. Res. Inv. Report.* 99–4259.

Paul A. (1982) Chemistry of Glasses. Chapman & Hall, London.

Perret D., Crovisier J. L., Stille P., Shields G., Mäder U., Advocat T., Schenk K. and Chardonnens M. (2003) Thermodynamic stability of waste glasses compared to leaching behaviour. *Appl. Geochem.*, in press.

AQ: 4

Petit J.-C. (1992) Natural analogues for the design and performance assessment of radioactive waste forms: a review. *J. Geochem. Explor.* **46,** 1–33.

Petit J.-C., Della Mea G., Dran J.-C., Magonthier M.-C., Mando P. A. and Paccagnella A. (1990) Hydrated-layer formation during dissolution of complex silicate glasses and minerals. *Geochim. Cosmochim. Acta* **54,** 1941–1955.

Plodinec M. J. and Wicks G. G. (1994) Application of hydration thermodynamics to in-situ test results. *Mater. Res. Soc. Symp. Proc.* **333,** 145–157.

Rowe G. L. Jr. and Brantley S. L. (1993) Estimation of the dissolution rates of andesitic glass, plagioclase and pyroxene in a flank aquifer of Poas Volcano, Costa Rica. *Chem. Geol.* **105,** 71–87.

Ruxton B. P. (1988) Towards a weathering model of Mount Lamington ash, Papua New Guinea. *Earth Sci. Rev.* **25,** 387–397.

Seyfried W. E. Jr. and Bischoff J. L. (1979) Low temperature basalt alteration by seawater: an experimental study at 70°C and 150°C. *Geochim. Cosmochim. Acta* **43,** 1937–1947.

Shoji S., Nanzyo M., Shirato Y. and Ito T. (1993) Chemical kinetics of weathering in young andisols from northeastern Japan using soil age normalized to 10°C. *Soil Sci.* **155,** 53–60.

Silber A., Bar-Yosef B. and Chen Y. (1999) pH-dependent kinetics of tuff dissolution. *Geoderma* **93,** 125–140.

Spivack A. J. and Staudigel H. (1994) Low-temperature alteration of the upper oceanic crust and the alkalinity budget of seawater. *Chem. Geol.* **115,** 239–247.

Staudigel H., Hart S. R., Schmincke H. and Smith B. M. (1989) Cretaceous ocean crust at DSDP site-4417 and site-418: Carbon uptake from weathering versus loss by magmatic outgassing. *Geochim. Cosmochim. Acta* **53,** 3091–3094.

Stumm W. and Morgan J. J. (1996) Aquatic chemistry. 3rd edition, Wiley and Sons, New York.

Techer I., Advocat T., Lancelot J. and Liotard J. M. (2001) Dissolution kinetics of basaltic glasses: Control by solution chemistry and protective effect of the alteration film. *Chem. Geol.* **176,** 235–263.

Tester J. W., Worley W. G., Robinson B. A., Grigsby C. O. and Feerer J. L. (1994) Correlating dissolution kinetics in pure water from 25 to 625°C. *Geochim. Cosmochim. Acta* **58,** 2407–2420.

Thompson G. (1983) Basalt-seawater interaction. In *Hydrothermal Processes at Seafloor Spreading Centers* (eds. P. A. Rona, K. Bostom, Laubier L. and Smith K. L.) pp. 225–278. Plenum Press, New York.

van den Bogaard P. and Schirnick C. (1995) $^{40}Ar/^{39}Ar$ laser probe ages of Bishop Tuff quartz phenocrysts substantiate long-lived silicic magma chamber at Long Valley, United States. *Geology* **23,** 759–762.

AQ: 5

White A. F. (1983) Surface chemistry and dissolution kinetics of glassy rocks at 25°C. *Geochim. Cosmochim. Acta* **47,** 805–815.

White A. F. and Claassen H. C. (1980) Kinetic model for the short-term dissolution of a rhyolitic glass. *Chem. Geol.* **28,** 91–109.

White A. F. and Peterson M. L. (1990) Role of reactive surface area characterization in geochemical kinetic models. In *Chemical modelling of aqueous systems II* (eds. Melchior and D. C. Bassett) pp. R. L. 461–475. ACS Symposium Series 416.

White A. F. and Brantley S. L. (2003) The effect of time on the weathering of silicate minerals: why do weathering rates differ in the laboratory and field? *Chem. Geol.* **202,** 479–506.

White A. F, Claassen H. C, Benson L. V (1980) The effect of dissolution of volcanic glass on the water chemistry in a tuffaceous aquifer, Rainier Mesa, Nevada. *U. S. G. S. Water Supply Paper.* 1535-Q.

White A. F., Blum A. E., Schulz M. S., Bullen T. D., Harden J. W. and Peterson M. L. (1996) Chemical weathering of a soil chronosequence on granitic alluvium: I. Quantification of mineralogical and surface area changes and calculation of primary silicate reaction rates *Geochim. Cosmochim. Acta* **60,** 2533–2550.

Wohletz K (2002) KWare Magma. http://internet.cybermesa.com/~wohletz/KWare.htm.

Wolff-Boenisch D., Gislason S. R. and Oelkers E. H. (2004) The effect of fluoride on the geometric surface area normalized dissolution rates of natural volcanic glasses at pH 4 and 25°C. *Geochim. Cosmochim. Acta*, in press.

AQ: 6

Yokoyama T. and Banfield J. F. (2002) Direct determinations of the rates of rhyolite dissolution and clay formation over 52,000 years and comparison with laboratory measurements. *Geochim. Cosmochim. Acta* **66,** 2665–2681.

AUTHOR QUERIES

AUTHOR PLEASE ANSWER ALL QUERIES **1**

AQ1— This reference is not cited in the text.

AQ2— Please update this reference

AQ3— Please update this reference.

AQ4— Please update this reference

AQ5— This reference is not cited in the text.

AQ6— Please update this reference